Optimal design of experiments for computing the fatigue life of an offshore wind turbine based on stepwise uncertainty reduction

Alexis Cousin, Nicolas Delépine, Martin Guiton, Miguel Munoz Zuniga, Timothée Perdrizet

Structural Safety 110 (2024) 102483

Contents lists available at ScienceDirect

Structural Safety

journal homepage: www.elsevier.com/locate/strusafe

Optimal design of experiments for computing the fatigue life of an offshore wind turbine based on stepwise uncertainty reduction

Alexis Cousin *, Nicolas Delépine, Martin Guiton, Miguel Munoz Zuniga, Timothée Perdrizet [1]

IFP Energies nouvelles, 1 et 4 avenue de Bois-Préau, Rueil-Malmaison, 92852, France

ARTICLE INFO

Keywords:
Active kriging
Fatigue damage
Offshore wind turbine
Stepwise uncertainty reduction
Bayesian quadrature
Expectation estimation

ABSTRACT

The design of an offshore wind turbine to resist fatigue damage during its whole service life requires to estimate an expectation over the pluri-annual joint statistics of wind and wave variables. Using a full factorial-based integration for the estimation of the cumulative fatigue damage represents a tremendous computational cost with aero-servo-hydro-elastic solvers which is generally not affordable by industrial designers. To overcome this limitation, strong approximations with lumping of environmental discretized joint probability (scatter diagram) are generally employed. We present in this paper a new method, called MAKSUR, involving the iterative enrichment of a design of experiments tailored to provide a good approximation of the long term mean damage. This method relies on a Kriging response surface with a learning criterion defined as the variance of the mean damage integral. It is compared to another previous similar approach called AK-DA, also dedicated to damage prediction, but is shown to converge more efficiently and with less numerical parameters to define by the user. The potential of the method for offshore wind turbine is demonstrated by a realistic 6D floating wind turbine case study with six wind and wave input variables.

1. Introduction

Offshore Wind is currently in active development and is expected to play a key role in transition to renewable energy, as illustrated by the 111 GW ambitious target for European Union [1], for the installed capacity of offshore wind power in the EU by 2030. To achieve this goal, a reduction of Levelized Cost of Energy (LCOE, sum of total cost divided by the sum of total energy produced over the installation lifetime) is required. A significant part of current LCOE is due to conservatism in Offshore Wind Turbine (OWT) design as a way to cope with epistemic uncertainty. OWT design must satisfy multiple limit states [2]: ultimate, fatigue, accidental, and serviceability for the various configurations of wind, wave, current loading, and also turbine states (operational or not). They represent several thousand costly aero-servo-hydro-elastics simulations [3]. Among these limit states, Fatigue Limit State (FLS) is specifically challenging for the numerical cost as it must sample the whole distribution of environmental loads which is expected to occur during the OWT service life. Indeed, FLS considers the mean expectation of damage over the environmental load distributions that may occur during service life (about 25 years for OWT). On top of efficiency, an accurate enough prediction is needed to reduce the high safety factor accounting for multiple uncertainties, specifically the uncertainty of maximum cycle laws from experimental tests and the uncertainty deriving from the assumption of independent loading events implied when using Palmer–Miner cumulative rule for damage [4,5].

Environmental loads of OWT, from winds, waves and currents are represented by finite number of parameters (see details in Section 3) with a joint distribution generally provided in discretized tables called scatter diagrams with only partial view of the correlation (e.g. projected on 2D plane for the wave significant height and wave peak period according to bins of standard deviation of wind speed and bins of directions as in [3,6]).

The current practice of OWT industrial designers is to compute FLS with a reduced discretized version of the input joint distribution by means of lumping of scatter diagrams blocks (also known as blocking), as illustrated by the 10 to 50 required number of sea states mentioned in [7]. However OWT standards like the latter or [8] based on [9] do not give details on the lumping strategy, excepted for the standard deviation of wind speed. Indeed, for the Normal Turbulence Model used in FLS design load cases DLC 1.2 and DLC 6.4, IEC [9] indicates that damage estimate over the standard deviation of wind speed distribution can be replaced by a representative value as the 90% quantile of the standard deviation of wind speed for a given time-averaged wind speed bin. Note however that Q90 was chosen representative for blade

* Corresponding author.
E-mail address: alexis.cousin@ifpen.fr (A. Cousin).
[1] Now affiliated to GreenWITS

https://doi.org/10.1016/j.strusafe.2024.102483
Received 12 July 2023; Received in revised form 20 May 2024; Accepted 20 May 2024
Available online 31 May 2024

composite material with high m exponent (typically ten to fourteen). For other OWT components, with steel material (m going from three to five), like the tower or some foundations, the Q90 would produce a too conservative fatigue estimate [10]. Traditional wave lumping methods from oil and gas engineering have used high quantile for the wave height, due to its direct relation to the wave amplitude, and to select few quantiles of wave period to account for more complex wave structure interaction. This should produce a conservative prediction of damage. However, the case of OWT and more specifically of floating ones is more complex due to interaction with aerodynamic loading, OWT controller in pitch and torque and OWT mechanical properties involved in dynamics as damping and stiffness [11]. This results in numerous possible resonance issues at initial stage of design with rotor harmonics which may not be well captured for damage estimate by too simplistic blocking [5,12].

Several lumping approaches dedicated to OWT have been suggested in the literature among which we distinguish that of Passon and Branner [6] which suggest use a lumping either on the wave height and wave period by computing a damage equivalent value in analogy to the Damage Equivalent Load. It has been later improved to consider the wind–wave correlation as presented in [12]. The latter computes, for each OWT component to design against FLS and for or a given bin of time-averaged wind speed, a contour when damage in the wave height and wave period joint space corresponds to a target damage computed with a full factorial analysis (during which the damage is evaluated at each point of a sample covering the joint space). One may also note other approaches to select a reduced number of variable sets according to their contribution to the total expectation of damage [13] or by means of statistical regression [14].

An increasingly popular family of methods used to face the computational limit, without the approximation of the lumping approaches, is that of surrogate modelling. This strategy aims at building, from a Design Of Experiments (DoE), an approximate function reproducing the results of the costly simulator with a low computational cost. A large variety of surrogates have been suggested among which popular ones are Polynomial Interpolation, Radial Basis Interpolation (RBI), Gaussian process modelling (GP) often known as Kriging, Support Vector, Polynomial Chaos Expansion (PCE) and Artificial Neural Network (ANN). Examples of application in prediction of long term mean fatigue of OWT can be found in [15] with PCE accounting for turbulence stochasticity, [16–18] with GP, [19] with RBI and [20] with ANN. Cons and pros can be considered for the choice of the most appropriate method, as discussed in several reviews [21–25]. A specific comparison between PCE and universal Kriging for reliability fatigue analysis of OWT is discussed in [26,27] and conclude to a higher accuracy of Kriging but with a higher computational cost which must be put into perspective with the cost of one or a batch of simulations. Whatever the chosen surrogate method, a particular attention must be paid on the model prediction quality in order to avoid poor representativity, overfitting or ill-conditioning if points of the DoE are too close. This is generally tested by means of bootstrap procedures with varying sample sizes and cross validation measures like leave-one-out [28,29].

Despite their interest for reducing the simulation cost of subsequent FLS, for instance when involved in a OWT design optimization, the common drawback of these methods is the need to compute first a full factorial analysis i.e. a costly surrogate construction independent to the final objective of mean damage estimation. To alleviate these limitations, multiple approaches have been suggested which aims at predicting the mean damage with a target accuracy but limiting as possible the number of calls to the simulator.

A first way would be to use Monte Carlo integration with an efficient sampling of the variable space, like the low-discrepancy quasi random sampling based on Sobol sequence used in [30]. A presentation and comparison of different sampling approaches including Latin Hypercube Sampling (LHS), Sobol and Hammersley Sequence sampling can be found in [31]. Dedicated solutions have been developed with surrogate models based on adaptive design of experiments (DoE) enrichment like for instance sparse PCE for failure probability estimation in [32]. Among the various surrogate strategies, GP is well suited for this iterative strategy as it provides by construction an estimate of the model error with the GP variance and for this main reason will be the one considered in this study. Note that GP models, with standard settings, are generally limited to a few dozen of dimensions, the bottleneck being the size of the learning set required which increases with the dimension [33].

When dealing with a surrogate of a numerical model output for estimating a post-process of the output (probability of exceedance, quantile, optimum, mean...), two potentially complementary learning strategies are possible: seek for precise surrogate prediction on the overall variable space and focus on sub-spaces important to the final post-processed quantity of interest. When possible, a compromise between this two strategies is often preferred. For GP, a list of Adaptive Kriging (AK) methods have been developed tailored to different post-processes of the surrogate such as: optimization [34], excursion set estimation [35,36], failure probability estimation [37], each with a dedicated criterion used to enrich the DoE and stopping condition. As a general rule, all criteria offer a compromise between exploration of the parametric space and exploitation of learned information important for the quantity of interest. A comparison of several criteria is given in the recent review [38].

In the context of expectation estimation, Bayesian Quadrature (BQ) is a well developed GP based method focused on generating a set of integration points optimal in terms of variance minimization [39]. This approach is not adaptive in the sense that it only depends on the integration point positions with respect to the probability distribution involved in the expectation and does not consider any model output evaluation as source of information. Equivalences and deep links with kernel herding [40] and space-filling designs can be found for instances in [41,42]. Complexity and rates of convergence of these strategies are also studied in [43,44]. In a very similar context to ours, Fekhari et al. [18] applied this optimal Bayesian quadrature strategy for the expected damage estimation of an OWT in a non-adaptive (in the previously defined sense) “one-shot” quadrature construction. This strategy presents the advantage to be fully parallelizable and decoupled with the simulation part which simplifies its implementation. Nevertheless, this type of strategy requires an un-informed initialization of the GP hyperparameters that could benefit from dedicated strategies such as in [45] and is by essence non-adaptive.

Also, of particular interest for us, Huchet et al. [46] has proposed a method, called Adaptive Kriging for Damage Assessment (AK-DA), dedicated to the computation of the long term expectation of fatigue damage (see details in the next sections). It provides a basis of comparison for a new method called MAKSUR suggested in this paper and which is formulated according to the Stepwise Uncertainty Reduction (SUR) principle [47].

SUR main idea is to select a new point which will minimize an expected uncertainty measure (often involving the GP posterior variance) when including this new point. In our work the uncertainty measure considered is the posterior expectation variance. For fixed GP hyperparameters our SUR approach is then completely equivalent to the optimal BQ one either with a “one shot” or sequential design construction. As will be presented, the main difference between our approach and BQ resides in the optimization of the hyperparameters that we achieve after each add of batch of integration points leading to a batch-sequential adaptive strategy. The optimization of the GP hyperparameters enables to capture information about the model output (partial annual damage d, see (1)) variability. The adaptive aspect of our approach also lies in the stopping criterion (coefficient of variation) of the DoE enrichment, which involves the available model output data.

This paper should be seen as a straightforward introduction of the SUR formalism for expectation estimation which introduce a natural

adaptive criteria that improves a known strategy (AK-DA) used in OWT reliability. Moreover the introduced SUR strategy has as particular case the mentioned non-adaptive BQ method used for instance in [18].

The content of this paper is the following. Section 2 gives the principles of AK-DA and MAKSUR adaptative kriging methods. Section 3 presents a Floating OWT (FOWT) case study inspired from the SBM Offshore/IFPEN TLP floater concept [48], with a generic 6 MW wind turbine and 6D wind and wave variable space, for a site in the East coast of United States [49]. Section 4 illustrates their application to a theoretical 2D (mean and standard deviation of wind speed only) case, with an artificial strongly non uniform damage distribution. Section 5 illustrates a more realistic application to the FOWT case study. Finally, conclusions and perspectives are given in Section 6.

2. Adaptive Kriging strategy for damage estimation

2.1. The general framework

Let X be a random vector taking values in $\Omega_X \subset R^{n_X}$ with known probability density function (pdf) f_X. It is composed of continuous random variables with finite variance. Let $d : \mathbb{R}^{n_X} \to \mathbb{R}^+$ be the short term partial annual damage occurring at a specific localization of the structure. The total annual damage D is defined as follows:

$$D = \mathbb{E}_X\left[d(X)\right] = \int_{\Omega_X} d(x) f_X(x) dx \tag{1}$$

where $\mathbb{E}_X$ is the expectation with respect to the distribution of X.

We can estimate D with the Monte Carlo method by considering a sample of X of size n_{MC} denoted $\mathbb{X}_{MC}$ leading to the following Monte Carlo estimator of D:

$$D_{MC} = \frac{1}{n_{MC}} \sum_{x \in \mathbb{X}_{MC}} d\left(x\right). \tag{2}$$

This estimation however necessitates n_{MC} evaluations of d which can be prohibitive when one evaluation of d requires one call to an expensive simulator. To avoid a large number of simulations, we implement in this paper an adaptive approach based on a surrogate model.

In this paper, the chosen surrogate model is a Kriging model [33, 50]. This technique consists in considering d as a realization of a stochastic process. The a priori distribution of this process is assumed to be stationary and Gaussian with autocorrelation function chosen by the user. The DoE, the evaluations of d at the DoE, and the Bayes' rule are then used to obtain the a posteriori distribution given the evaluations of the model at the initial DoE. This a posteriori process, denoted $\widetilde{d}$, remains a Gaussian process whose mean and autocorrelation function can be analytically computed (see Appendix A for more detail). Thus, at each point $x \in \Omega_X$, the Kriging model provides a prediction of $d(x)$ in the form of a Gaussian random variable with mean $\mu(x)$ and variance $\sigma(x)^2$. In particular for any $x, x' \in \Omega_X$, from the stationarity hypothesis, the posterior covariance is only a function of x and x' and therefore in the sequel will be referred to as $c(x, x')$. The mean function μ is used as predictor while the standard deviation function σ measures the accuracy of the predictor. This surrogate model technique is particularly well suited for small dimension problem (when n_X is small) and for a sequential strategy since σ enables to identify areas where the surrogate model needs to be refined.

The Kriging random version of the total damage

$$\widetilde{D} = \int_{\Omega_X} \widetilde{d}(x) f_X(x) dx \tag{3}$$

is a Gaussian random variable (see for instance 35) with known mean $\mu_{\widetilde{D}} = \mathbb{E}_X[\mu(X)]$ and variance $\sigma^2_{\widetilde{D}} = \mathbb{E}_{X,X'}[c(X, X')]$, with X' a random variable independent and identically distributed as X, or more explicitly:

$$\sigma^2_{\widetilde{D}} = \int_{\Omega_X} \int_{\Omega_X} c(x, x') f_X(x) f_X(x') dx dx'. \tag{4}$$

The Monte Carlo random estimator of D based on the surrogate model is given by

$$\widetilde{D}_{MC} = \frac{1}{n_{MC}} \sum_{x \in \mathbb{X}_{MC}} \tilde{d}\left(x\right). \tag{5}$$

Since $\widetilde{d}$ is a Gaussian process, $\widetilde{D}_{MC}$ is also a Gaussian random variable with mean and variance given by

$$\widetilde{\mu}_{MC} := \mathbb{E}\left[\widetilde{D}_{MC}\right] = \frac{1}{n_{MC}} \sum_{x \in \mathbb{X}_{MC}} \mu(x) \tag{6}$$

and

$$\widetilde{\sigma}^2_{MC} := \mathrm{Var}\left(\widetilde{D}_{MC}\right) = \frac{1}{n^2_{MC}} \sum_{x \in \mathbb{X}_{MC}} \sum_{x' \in \mathbb{X}_{MC}} c\left(x, x'\right). \tag{7}$$

Since the surrogate $\widetilde{d}$ is fast to evaluate, the MC sampling $\mathbb{X}_{MC}$ is considered large enough for the approximation error between the two random variables $\widetilde{D}$ and $\widetilde{D}_{MC}$ to be negligible. Note that the integration error could naturally (according to the central limit theorem) be modelled as a centred Gaussian variable, added to D_{MC}, with a variance of order of magnitude $1/n_{MC}$. Another equivalent way to account for the integration error would be to consider a noisy GP with noise variance estimated jointly with the other hyperparameters. In the rest of the article the integration error is considered negligible and only the GP epistemic uncertainty will be dealt with.

In this introduced framework we implement the following active kriging strategy. First, a DoE composed of n_0 points of Ω_X is created and denoted $\mathbb{X}^0_d$. The expensive function d is then evaluated at each point of $\mathbb{X}^0_d$. The results are used to build an approximation model of d called surrogate model and denoted $\widetilde{d}$. To improve the accuracy of this surrogate model, an enrichment procedure composed of cycles of enrichment is then carried out. An enrichment cycle aims at selecting new points of Ω_X where the fitting of the surrogate model must be improved. The expensive function d is then evaluated at each of the enrichment points and the surrogate model is updated. At the end of the enrichment procedure, the quantity of interest D_{MC} can then be estimated simply by replacing d with the updated surrogate model predictor, without additional simulations. The AK strategy is summarized in Algorithm 1.

Algorithm 1 AK strategy

Build the initial DoE: $\mathbb{X}^0_d$
Calibrate the initial Kriging model of d from $\mathbb{X}^0_d$: $\widetilde{d}$
$k \leftarrow 0$ ▷ number of enrichment cycles
while the stopping condition is not met **do**
  selection of the enrichment points: select n_{enr} points of Ω_X using one of the approaches described in Sections 2.2, 2.3, and 2.4
  Evaluate d at the new points ▷ requires n_{enr} simulations
  Update the DoE and use it to recalibrate the Kriging model
  $k \leftarrow k + 1$
end while
Provide the statistical estimator $\widetilde{D}_{MC}$ of D given in (5) where $\widetilde{d}$ is the Kriging model calibrated from the updated DoE.
As estimation for D use for instance $\widetilde{\mu}_{MC}$ in (6) or any desired quantile.

The parameter n_{enr} corresponding to the number of points added during each cycle of enrichment to the DoE is chosen by the user. When $n_{enr} = 1$, the enrichment is said sequential and the enrichment is said multipoint when $n_{enr} > 1$.

The stopping condition of the adaptive procedure considered in this paper involves the coefficient of variation of $\widetilde{D}_{MC}$ defined as follows:

$$C.o.V_{MC} = \frac{\widetilde{\sigma}_{MC}}{\widetilde{\mu}_{MC}}. \tag{8}$$

The stopping condition is met when, at the end of a cycle of enrichment, $C.o.V_{MC}$ is below some threshold chosen by the user. Other

stopping conditions can be considered such as the maximum number of cycles of enrichment.

In the following sections, we describe three approaches to perform the selection of the enrichment points: an uncorrelated (meaning it does not take into account the correlations of $\widetilde{d}$ between MC sample points) approach, the method suggested in [46] called AK-DA, and finally, a method introduced in this paper: MAKSUR. The AK strategy described in Algorithm 1 will then be applied on two test cases with the three different enrichment approaches to compare their performance.

At the beginning of the kth cycle of enrichment, we have $\mathbb{X}_d^{k-1}$ the DoE resulting from the $(k-1)$-th cycle. We denote $\mathbb{X}_c$ the set of candidate points for the enrichment and $\mathbb{X}_{enr}$ the enrichment points selected during the current cycle of enrichment.

2.2. A reference heuristic enrichment criterion

For the uncorrelated approach, we introduce only the sequential enrichment in this paper. Here, the selection of the enrichment point is performed by solving Eq. (9):

$$x_{enr} = \underset{x_c \in \mathbb{X}_c}{\operatorname{argmax}} \mu(x_c) \times \sigma(x_c) \times f_X(x_c) \tag{9}$$

where $\mathbb{X}_c = \mathbb{X}_{MC}$. At the end of the kth cycle of enrichment, $\mathbb{X}_{enr} = \{x_{enr}\}$.

Thus, the uncorrelated approach aims at selecting among the Monte Carlo sample of X a point x_c where the prediction of the partial damage $\mu(x_c)$, the uncertainty of prediction $\sigma(x_c)$, and the probability of occurrence $f_X(x_c)$ are large.

Algorithm 2 k-th enrichment cycle with the sequential uncorrelated approach

Select x_{enr} solution of equation:

$$x_{enr} = \underset{x_c \in \mathbb{X}_c}{\operatorname{argmax}} \mu(x_c) \times \sigma(x_c) \times f_X(x_c)$$

$$\mathbb{X}_d^k \leftarrow \left\{\mathbb{X}_d^{k-1}, \mathbb{X}_{enr}\right\}$$

2.3. The AK-DA enrichment criterion

The AK-DA approach aims at selecting the points from the Monte Carlo sample which contribute the most to $\mathrm{Var}\left(\widetilde{D}_{MC}\right)$ given in Eq. (7). To do so, the selection of the n_{enr} enrichment points in Algorithm 1 is performed in an iterative way. During each iteration, the selected enrichment point x_{enr} is the candidate with the larger contribution to $\mathrm{Var}\left(\widetilde{D}_{MC}\right)$:

$$x_{enr} = \underset{x_c \in \mathbb{X}_c}{\operatorname{argmax}} \left| \sum_{x' \in \mathbb{X}_{MC}} c\left(x_c, x'\right) \right|. \tag{10}$$

During the first iteration, $\mathbb{X}_c = \mathbb{X}_{MC}$. At the end of each iteration, once the enrichment point x_{enr} is selected, the set of candidates $\mathbb{X}_c$ is updated by keeping only the points x_c such that $\widetilde{d}(x_c)$ is weakly correlated with $\widetilde{d}(x_{enr})$ (i.e. such that $\left|c\left(x_c, x_{enr}\right)\right| \leq r$ where r is a parameter chosen by the user). This parameter r has a major impact on the procedure since it eliminates the candidates for enrichment which are too close to x_{enr}. It thus avoids having two enrichment points very close together and providing no further information. However, this parameter r must be chosen by the user and is not easy to define a priori.

This way, the enrichment points selected during a cycle of enrichment have a large contribution in $\mathrm{Var}\left(\widetilde{D}_{MC}\right)$ and the information provided by the evaluation of d at these points is not redundant.

The AK-DA approach is summarized in Algorithm 3.

In [46], AK-DA is introduced by evaluating the total damage from a regular grid of long term variables which is suited for a small dimension n_X. In this paper, a Monte Carlo approach is preferred and therefore, the AK-DA enrichment is slightly modified accordingly.

Algorithm 3 k-th enrichment cycle with multipoint AK-DA approach

$\mathbb{X}_c \leftarrow \mathbb{X}_{MC}$, $\mathbb{X}_{enr} \leftarrow \emptyset$
$i \leftarrow 0$
while $i < n_{enr}$ or $\mathbb{X}_c \neq \emptyset$ **do**
  Select x_{enr} solution of Eq. (11)

$$x_{enr} = \underset{x_c \in \mathbb{X}_c}{\operatorname{argmax}} \left| \sum_{x' \in \mathbb{X}_{MC}} c\left(x_c, x'\right) \right| \tag{11}$$

  $\mathbb{X}_{enr} \leftarrow \{\mathbb{X}_{enr}, x_{enr}\}$
  $\mathbb{X}_c \leftarrow \left\{x_c \in \mathbb{X}_c \text{ such that } \left|c\left(x_c, x_{enr}\right)\right| \leq r\right\}$
  $i \leftarrow i + 1$
end while
$\mathbb{X}_d^k \leftarrow \left\{\mathbb{X}_d^{k-1}, \mathbb{X}_{enr}\right\}$

Contrary to the original AK-DA criterion, the modified version we suggest with a Monte Carlo estimation does not require to know the distribution of the long-term variables. Only a Monte Carlo sample is required, which in practice is given directly from the measurement of wind and wave statistics. We thus avoid the fitting of a parametric distribution and its related uncertainty [51]. This remark holds as well for the MAKSUR criterion introduced below.

2.4. Active Kriging based on a Stepwise Uncertainty Reduction approach for mean estimation

The new enrichment approach introduced in this paper is called MAKSUR for Mean estimation with AK based on Stepwise Uncertainty Reduction. It aims at selecting the design point(s) that will theoretically minimize, w.r.t. a new design point, the expected posterior variance of $\widetilde{D}$ given the values of damage d at the selected design point.

Sequential enrichment.

Since $\widetilde{D}$ is the integrated damage estimated with a GP model as integrand, the uncertainty on $\widetilde{D}$ is epistemic and derived from the GP model uncertainty through the integration. For a DoE of size M, we would like to find the couple $(x_{M+1}, d(x_{M+1}))$ to add to the GP learning DoE such that the uncertainty on $\widetilde{D}$, with the upgraded GP model, is reduced. The uncertainty measure considered is the variance and since the integrand value $d(x_{M+1})$ is unknown at this point, it is replaced with its GP posterior prediction. The selection criteria is then defined by considering the expected variance of $\widetilde{D}$ w.r.t the GP posterior prediction at x_{M+1}. In practice the posterior variance of the MC estimator $\widetilde{D}_{MC}$ is considered, leading to the following optimal selection of a design point candidate x_{M+1} such that:

$$x_{M+1} = \underset{x_c \in \mathbb{X}_{MC}}{\operatorname{argmin}} \mathbb{E}_{\tilde{d}(x_c)}\left[\mathrm{Var}\left(\widetilde{D}_{MC} \middle| \tilde{d}(x_c)\right)\right] \tag{12}$$

In this sequential setting, with one enrichment point added at each iteration and fixed hyperparameters, the variance term can be explicitly formulated as

$$\mathrm{Var}\left(\widetilde{D}_{MC} | \tilde{d}(x_c)\right) = \frac{1}{n_{MC}^2} \sum_{x \in \mathbb{X}_{MC}} \sum_{x' \in \mathbb{X}_{MC}} \left[c(x, x') - \frac{c(x_c, x) c(x_c, x')}{c(x_c, x_c)}\right], \tag{13}$$

with c the current posterior covariance function (built with the DoE of size M) which explicit expression is given by (29) in the appendix. We can notice that the variance term (13) does not involve the posterior Gaussian prediction $\tilde{d}(x_c)$ but only x_c. Therefore in this particular SUR setting, the expectation in (12) can be removed. From simple manipulations on (13) the optimal design point selection boils down to

$$x_{M+1} = \underset{x_c \in \mathbb{X}_{MC}}{\operatorname{argmax}} \frac{1}{\sigma(x_c)} \left| \sum_{x' \in \mathbb{X}_{MC}} c\left(x_c, x'\right) \right|. \tag{14}$$

Multipoint enrichment.

Formulas for multipoint enrichment by batches are also available with MAKSUR from GP update formulas introduced in [52]. Nevertheless, this latter strategy involves a NP-hard, non-linear, multivariate optimization problem that can be very difficult to tackle [53]. In practice, as also pointed out in [53], a sub-optimal greedy version of the batch optimization problem can be preferred consisting in adding iteratively one point at a time. Indeed, this latter strategy is much easier to implement and involves a less complex optimization problem to solve at each iteration. The iterative version will be presented below and used in the numerical section.

Let us consider a cycle of n_enr enrichments with $\mathbb{X}_{enr} = \{x_{(enr,1)}, \dots, x_{(enr,n)}\}$ the set of n enrichment points already selected during this cycle. The $(n+1)$th enrichment point is the solution of the following problem:

$$x_{(enr,n+1)} = \underset{x_c \in \mathbb{X}_{MC}}{\operatorname{argmin}} \operatorname{Var}\left(\widetilde{D}_{MC} | \mathbb{D}_{x_c}\right) \tag{15}$$

where $\mathbb{D}_{x_c} = \{\widetilde{d}(y), y \in \{x_c, \mathbb{X}_{enr}\}\}$. Indeed, as shown in [52] and discussed previously in the sequential case with $n_{enr} = 1$ (Eq. (12) and (13)), for fixed hyperparameters, we can compute the posterior variance of $\widetilde{D}_{MC}|\mathbb{D}_{x_c}$ from the set of design points $\{x_c, \mathbb{X}_{enr}\}$ and without knowing the values of $\widetilde{d}$ on $\{x_c, \mathbb{X}_{enr}\}$. Similarly to the sequential case, the criteria does not need an expectation w.r.t. the posterior predictions. We refer to Appendix B for the computation of $\operatorname{Var}\left(\widetilde{D}_{MC}|\mathbb{D}_{x_c}\right)$ using only the covariance function of $\widetilde{d}$ and the set of design points $\{x_c, \mathbb{X}_{enr}\}$ leading to the equivalent optimization problem

$$x_{enr,n+1} = \underset{x_c \in \mathbb{X}_{MC}}{\operatorname{argmax}} \left(a_1, \dots, a_n, a_{x_c}\right)^T \Sigma^{-1}_{\mathbb{D}_{x_c}} \left(a_1, \dots, a_n, a_{x_c}\right) \tag{16}$$

where $a_i = \sum_{x \in \mathbb{X}_{MC}} c(x_{(enr,i)}, x)$, $a_{x_c} = \sum_{x \in \mathbb{X}_{MC}} c(x_c, x)$ and $\Sigma_{\mathbb{D}_{x_c}}$ given by (32) in Appendix B. To summarize, the problem (16) is solved n_{enr} time (total number of desired enrichment points) by updating the objective as formalized. The whole enrichment procedure does not require any costly evaluation of the simulator function $d(\cdot)$. The n_{enr} simulations are launched in batch after the enrichment cycle. The sequential enrichment can be seen as the particular case of the multipoint one when $n_{enr} = 1$.

The MAKSUR approach is summarized in Algorithm 4.

Algorithm 4 k-th enrichment cycle with multipoint MAKSUR approach

$\mathbb{X}_{enr} \leftarrow \emptyset$
$i \leftarrow 0$
while $i < n_{enr}$ **do**
  Select x_{enr} according to Eq. (16)
  $\mathbb{X}_{enr} \leftarrow \{\mathbb{X}_{enr}, x_{enr}\}$
  $i \leftarrow i + 1$
end while
$\mathbb{X}_d^k \leftarrow \left\{\mathbb{X}_d^{k-1}, \mathbb{X}_{enr}\right\}$

Discussion.

The MAKSUR approach has several advantages compared to AK-DA:

- with MAKSUR, it is not required to provide the parameter r which influences the performance of AK-DA.
- with AK-DA, the size of candidate set decreases with each iteration which can lead to an empty set $\mathbb{X}_c$ before the n_{enr}-th iteration. Therefore, during this last cycle, less than n_{enr} enrichment points are selected. This can result in a sub-optimal use of the computer resources (for instance if n_{enr} calculations can be carried out in parallel). With MAKSUR, during each cycle of enrichment, n_{enr} points are always selected.
- for $n_{enr} = 1$, the criteria (14) gives a theoretical validation to the covariance based criterion (10) introduced for AK-DA in [46] corrected in MAKSUR with the appropriate factor $1/\sigma(x_c)$. Indeed according to (10), the AK-DA criterion selects points strongly positively (or negatively) correlated with the MC sampling set (absolute sum term) enabling optimal global variance improvement. Meanwhile, according to (14), MAKSUR criterion encompasses the AK-DA one (absolute sum term) but additionally favours less uncertain points i.e. with small posterior variance (via factored term) further enhancing the expected variance minimization.

In [46], the enrichment points of AK-DA are selected from the grid used to evaluate the damage. For fair comparisons, enrichment candidates in the three approaches mentioned in the present paper are considered from the Monte Carlo sample used to estimate the damage. However, this enrichment strategy could benefit from using an optimization algorithm to select enrichment points from the entire domain Ω_X.

2.5. Illustration of an enrichment step using MAKSUR and AK-DA

To illustrate the enrichment procedure using the AK-DA and MAKSUR criteria, let us consider a simple 1D case. Let X be a uniform random variable on $[0, 2\pi]$ from which we draw a Monte Carlo sample. We consider $d(x) = 1.25x + \sin(3x)$ and we train an initial kriging model from a DoE composed of four points (see Fig. 1). We then compute the AK-DA and MAKSUR criteria (with respectively Eqs. (11) and (16)) for every point of the Monte-Carlo sample and display it in Fig. 1. The enrichment point for each criterion is the one maximizing it. They are denoted x_{AKDA} and x_{MAKSUR}.

The enrichment point x_{MAKSUR} is added to the initial DoE and a new kriging model is trained from this new DoE. The same operation is done with x_{AKDA}. The resulting kriging models are displayed in Fig. 2.

From each kriging model, we can estimate the total damage $\tilde{D}$ and display it in Fig. 3. These total damage estimations are normal random variables since we consider the uncertainty of the kriging. The means and variances of these variables are given by Eqs. (6) and (7). We observe that the estimations of the total damage has been improved with the enrichment step: the mean of the distributions are closer to the reference damage computed with Eq. (2). Moreover, we also observe that the variance of the total damage using the MAKSUR criterion is smaller than the initial one and the one using the AK-DA criterion. Indeed the MAKSUR criterion aims at selecting the point that minimizes the expected variance of the total damage estimated with the new kriging model i.e. the one enriched with a new design point (given by Eq. (15)) while AK-DA selects the point which contributes the most to the variance of the initial total damage estimated with the current kriging model. For fixed hyperparameters and after enrichment with respective criteria, the MAKSUR variance is necessarily smaller than the AK-DA one as illustrated in Fig. 3.

3. A 6D floating wind turbine case study based on an ANN of fatigue damage at the top of a mooring line

3.1. Wind and wave parameters

For FLS, wind speed process is assumed Gaussian and stationary on ten minutes, while the wave elevation process is also Gaussian but stationary on one to three hours. Designers generally start with historical wind and wave data over several years collecting measurements on met-masts and buoys, eventually completed with other sources by means of Measure-Correlate-Predict strategies (cf appendix F of 9). From historical data, one may compute joint probabilistic distribution of wind and wave random parameters, by means of parametric or non parametric fitting methods. The results will always include an uncertainty [51] which can be large when it is extrapolated for the OWT service life of the order of 25 years. The wind and wave random parameters generally considered in the literature to represent each stationary state are given in Table 1.

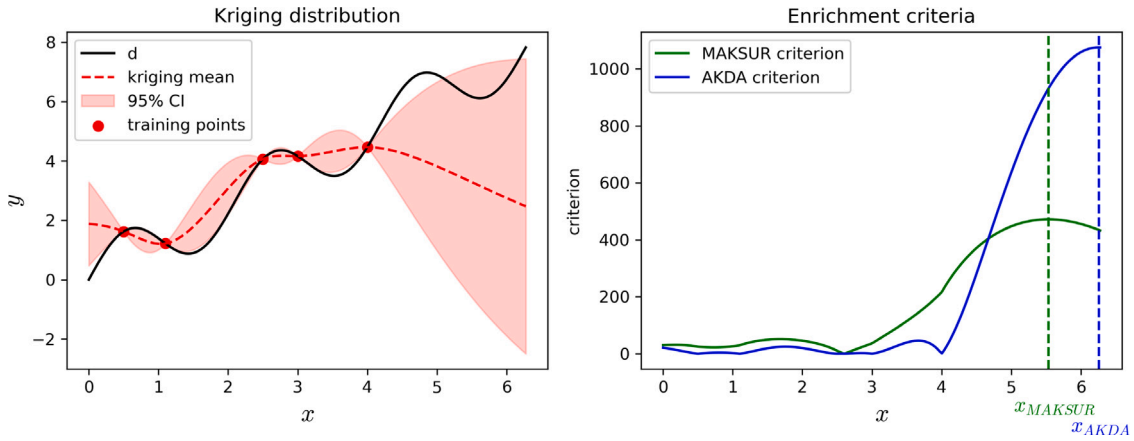

Fig. 1. Initial kriging model (left) and enrichment criteria (right).

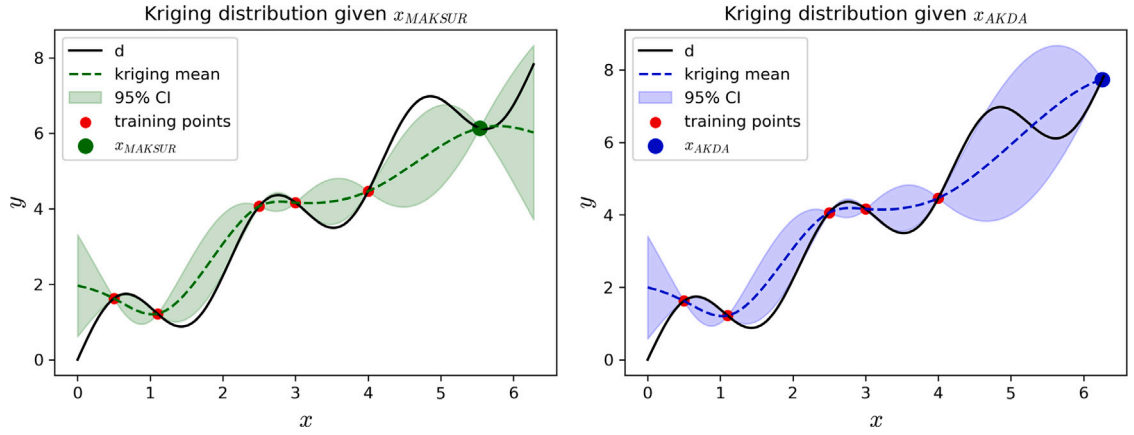

Fig. 2. Enriched kriging models using MAKSUR (left) and AKDA (right).

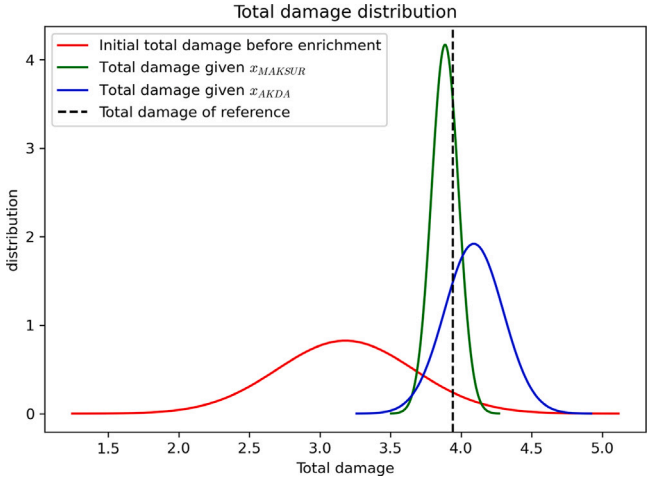

Fig. 3. Estimation of the total damage using the initial and enriched kriging models.

One may also consider additional variables like a coefficient of vertical shear for a wind profile in relation to the atmospheric stability [54], misalignment of the rotor, additional loading on the structure with submarine currents, marine growth, or multiple sets of wave components to describe the superposition of several sea states (e.g. wind sea and swell). We will however limit to the six above mentioned variables in this paper, the method presented being easily extendable to additional variables, up to the curse of dimensionality, with some limitations

Table 1
Wind and wave stationary state variables. In the first column abbreviations used in Fig. 6 are between brackets.

Variable	Description	Unit
U	Time-averaged wind speed at hub height	(m/s)
σ_U	Standard deviation of wind speed at hub height	(m/s)
θ_{wind} (WDIR)	Wind heading	(degree)
H_s (WVHT)	Wave significant height	(m)
T_p (DPD)	Wave peak period	(s)
θ_{wave} (MWD)	Wave heading	(degree)

detailed below. Let us denote X a random vector collecting all these environmental site variables.

3.2. Floating offshore wind turbine case study

We are interested in analysing the performance of the different AK criterion presented in Section 2 to compute efficiently the long term fatigue damage of a FOWT. In this perspective, we selected a realistic case study with a generic six MW wind turbine supported by a SBM Offshore/IFPEN TLP floater concept depicted in Fig. 4, which is derived from the concept presented in [48].

The site conditions are extracted from the station 4408 of a USA National Data Buoy Center which is located near Nantucket on the East coast of USA. A total of 60 673 sextuplet (U, σ_U, θ_{wind}, H_s, T_p, θ_{wave}) have been considered from recorded time period between 2007–2017, with 8-min statistic for the wind and 20-min statistics for the wave. Note that wind conditions are provided at buoy depth and

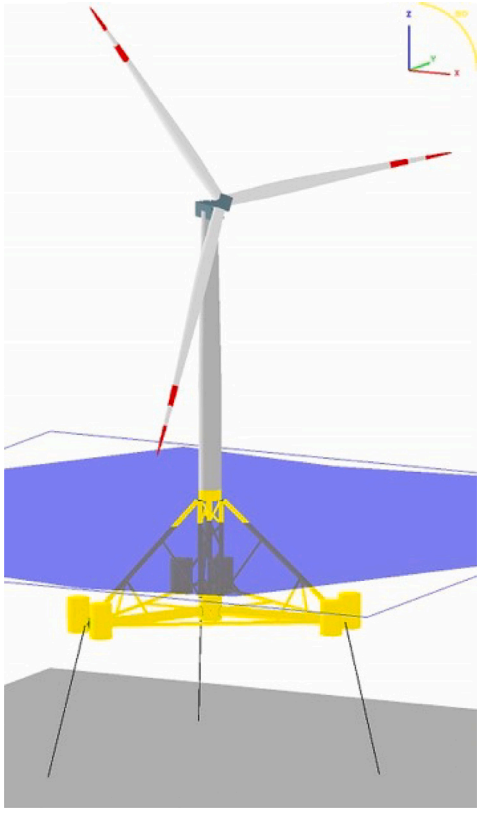

Fig. 4. 3D view of the FOWT with SBM Offshore/IFPEN TLP floater concept after [49].

Table 2
Marginal fitting distributions according to the offshore Nantucket buoy data. Γ and I_0 are the gamma function and the modified Bessel function of order 0, respectively.

Data	Distribution	pdf
U	Weibull(μ, λ, k)	$k\left(\frac{x-\mu}{\lambda}\right)^{k-1} e^{-\left(\frac{x-\mu}{\lambda}\right)^{k}}, x > 0$ $0,\ x \leq 0$
H_s, T_p	Gamma(μ, λ, k)	$\frac{1}{\Gamma(k)}\left(\frac{x-\mu}{\lambda}\right)^{k-1} e^{-\left(\frac{x-\mu}{\lambda}\right)}$
$\theta_{wind}, \theta_{wave}$	Von Mises(μ, λ, k)	$\frac{1}{2\pi I_0(k)} e^{k\cos\left(\frac{x-\mu}{\lambda}\right)}$

Table 3
Marginal fitting parameters defined in Table 2.

Data	μ	λ	k
U	−0.16 m/s	7.11 m/s	1.85
H_s	0.28 m	0.66 m	2.16
T_p	1.45 s	0.70 s	9.69
θ_{wind}	−1.92 rad	1 rad	0.31
θ_{wave}	2.71 rad	1 rad	1

should be higher at wind turbine hub height, depending on the vertical profile (wind shear) of the site. This correction was not taken into account in [49]. Joint distribution were fitted against this buoy data with python Scipy.stats package, for the marginal distributions of U, θ_{wind}, H_s, T_p, θ_{wave}, with results given in Tables 2 and 3.

The turbulence standard deviation σ_U is not provided in the buoy data so that a log-normal distribution is considered, after the suggestion of IEC [9] with following mean and standard deviation for a class C low turbulence :

$$\begin{aligned} \mathbb{E}\left[\sigma_U|U\right] &= 0.09U + 0.456 \\ \mathrm{Var}\left(\sigma_U|U\right) &= 0.168^2 \end{aligned} \tag{17}$$

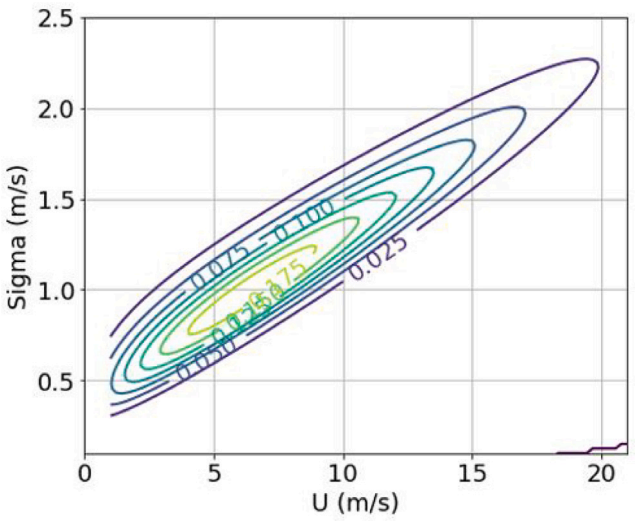

Fig. 5. pdf of the $\sigma_U - -U$ distribution.

where quantities are given in m/s. This joint probability is illustrated in Fig. 5.

Given the dominant role of time-averaged the wind speed U on the wind turbine mechanical behaviour, an hybrid strategy has been considered in [49], with an imposed sampling on that dimension and a LHS sampling over the left 5D, for each imposed U. The sampling along U is chosen between cut in and cut out steady wind speed every two metre per second, plus two additional points near the rated speed, defining a total of thirteen U points. The rated wind speed corresponds to a drastic change in the characteristic curves of the wind turbine (aerodynamic thrust and torque, electrical production) in steady regime, due to a change in the blade and the generator torque controller (see e.g. 55 for details on wind turbine behaviours and controller).

Thanks to a specific test on the new supercomputer Jean Zay owned by GENCI, IDRIS and CNRS (the most powerful one dedicated to research in France), it was possible to sample intensively the full 6D domain, with 20 000 points of a maximin LHS for each time-averaged wind speed imposed value. The total of 260 000 computations represents a greater sampling effort than previous works in the literature [27,30]. As damage of an OWT is the result of a multiphysics process, its long term expectation may be better approximated with a sampling of computations that is defined according to the input variables joint distribution. Several ways are suggested to define such sampling based on the representation of the correlation with either an a priori parametric 2D dependencies [56] or non parametric copulas [57]. In [49], the specific case of wind turbulence is using the parametric definition of Eq. (17) by sampling on the unit square and then use the inverse of the Cumulative Density Function (CDF) of the lognormal distribution to transform in the physical space. For the other 4D (θ_{wind}, H_s, T_p, θ_{wave}), the choice was to follow the methodology in [58] which requires only correlation matrices. As shown in Fig. 6, the first step is to define the LHS for 4 independent variables with standard normal distributions. Second step is to multiply the LHS matrix (20 000 x 4) with the empirical correlation matrix after triangulation by means of Cholesky factorization. The last step uses inverse of CDF to convert the sampling into the space of chosen distributions mentioned previously. The resulting sample points provide a good approximation of the empirical correlation as can be seen in Fig. 7.

Each sextuplet of environmental parameters is representing a x value (see Section 2) and is used to generate a set of wind and wave loading and to simulate one hour of the lifetime of a FOWT with dedicated Deeplines Wind^{TM} software. This length of simulation is

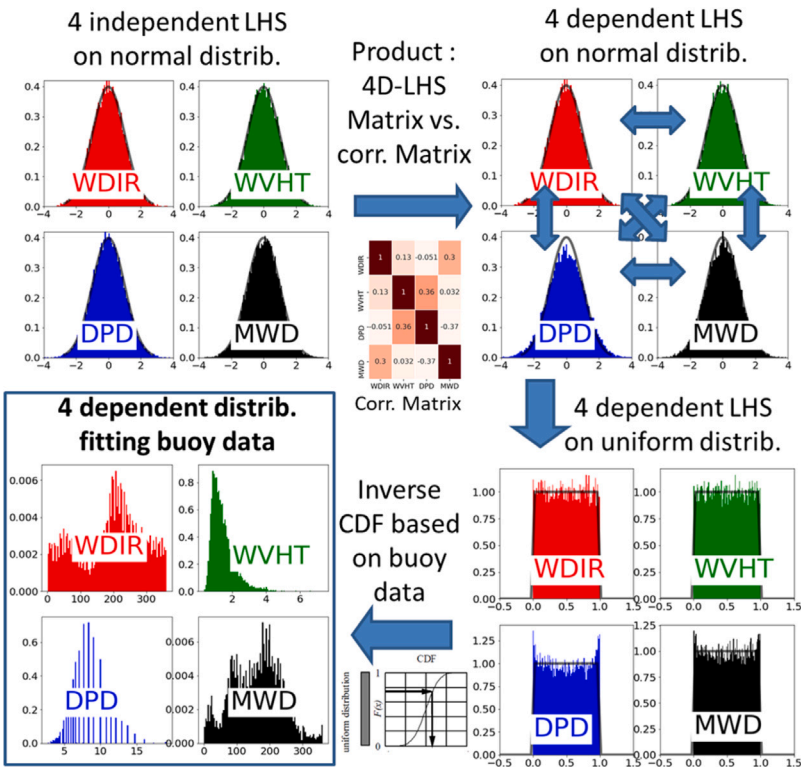

Fig. 6. Methodology of Zang and Pinder [58] to generate a LHS according to the 4 input variables with their correlation, after [49]. WDIR, WVHT, DPD and MWD correspond respectively to θ_{wind}, H_s, T_p and θ_{wave}.

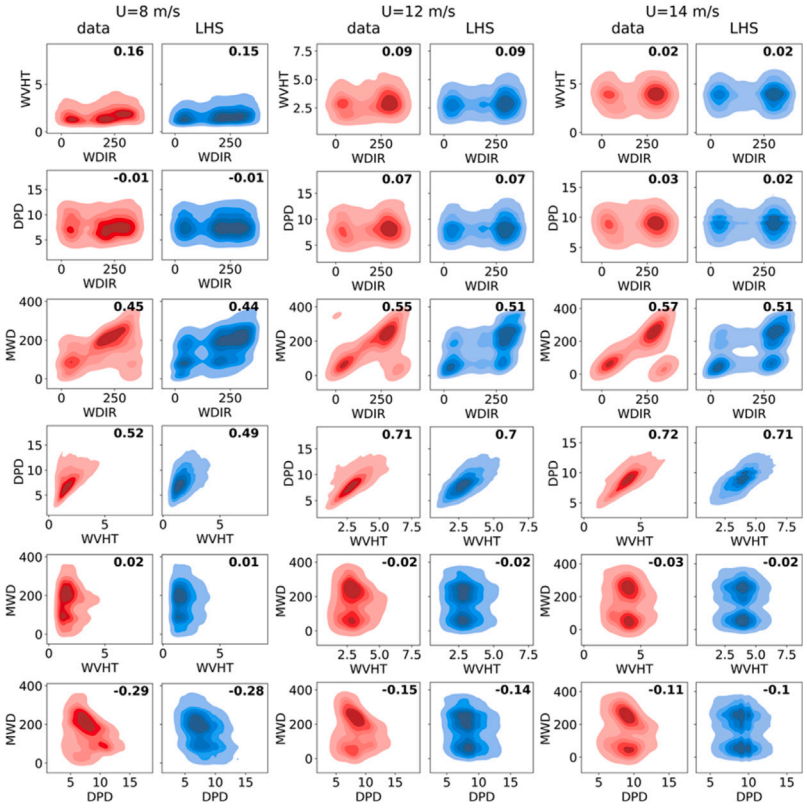

Fig. 7. 2D-Comparisons between Kernel Density Estimation of the buoy data with obtained LHS for U = 8, 12 and 14 m/s, after [49].

considered long enough to sample the main frequencies of both wind and wave Gaussian processes. Finally, a post-treatment of the damage $d(x)$ (see Eq. (2)) at the top of one of the three mooring lines is done. It is assumed that 1 h is also long enough to get a small enough

variance of $d(x)$, in agreement with the conclusions of the sections 4.3.2 of Müller et al. [59] for two FOWT case studies. The interested reader may also found a detailed study of the convergence of fatigue prediction according to simulation length, for a fixed foundation OWT case study in [60].

Consequently, there is no need to use several stochastic replications. The Rainflow cycle counting which is described in [61] and implemented in [62], is applied to the time series of the tension $T(t)$ at the top of the selected mooring line. The result of this algorithm is a collection of n tension ranges δT_i with i ranging from 1 to n, and the associated number of cycles n_i. An experimental and confidential fatigue law is then used to relate each tension range to a cycle Number N_i corresponding to damage rupture (see e.g. 63 for examples of such fatigue laws). The short-term partial damage is then computed as the ratio :

$$d(x) = \sum_{i}^{n} \frac{n_i}{N_i}. \tag{18}$$

The computation of the long term annual damage D of Eq. (1) from the Deeplines Wind™ simulations is achieved in two steps. For each U, we assume the 20 000 samples according to (σ_u, θ_{wind}, H_s, T_p, θ_{wave}) to be large enough and built according to the joint distribution so that it is equivalent to a MC integral (Eq. (2)) on that sub-space. Then the thirteen conditional expectations $\mathbb{E}[d(X)|U]$ values are integrated over the Weibull pdf of time-averaged the wind speed U. The resulting reference annual damage is :

$$D_{ref} = 0.008344 \tag{19}$$

3.3. ANN surrogate models in 2D and 6D

The cost of a single one hour aero-servo-hydro-dynamic simulation with Deeplines Wind™ is about ten hours of computation. To facilitate applications on this case study of several AK methods that will be documented in the next sections, two surrogate models which are fast to run are computed with ANN.

A reduced 2D problem ($d : \mathbb{R}^2 \to \mathbb{R}^+$) is considered for a first simplified application (see Section 4), with only U and σ_U input variables. The Multi-layer Perceptron Regressor method of sklearn.neural_network python package is applied on a set of 150 Deeplines Wind™ simulation results. The ANN options are 100 neurons in two hidden layers and rectified linear unit function (i.e. $\max(0, x)$) as activation functions. The cross validation of this 2D ANN has been checked on a validation DoE and is satisfying as can be seen Fig. 8.

For the full dimensional problem ($d : \mathbb{R}^6 \to \mathbb{R}^+$), the same methodology has been applied on the whole set of 260 000 simulation results. The quality of this 6D ANN is also satisfying, as shown by Fig. 9 despite a wider dispersion around the diagonal in particular for the smallest values (which might be due to a more complex input–output relation in this area). The contribution of these small damage points to the long term mean annual damage should however be small.

Finally, both neural networks are trained on $\log(d)$ which explains why the values of y_predict and y_test in Figs. 8 and 9 are negative.

4. Application to a 2D simplified case study

4.1. Description of the 2D case study

A first application is carried out by simplifying the 6D case study of the fatigue at the top of a mooring line described in Section 3 to a 2D problem. Indeed, in this section we will neglect the wave and orientation pluri-annual variables, to keep only time-averaged the wind speed U and the standard deviation of wind speed σ_U. For the sake of simplifications, the computational cost is drastically reduced by replacing the multiphysics simulator (Deeplines Wind™) by the 2D ANN presented in Section 3. Furthermore, to test the robustness of

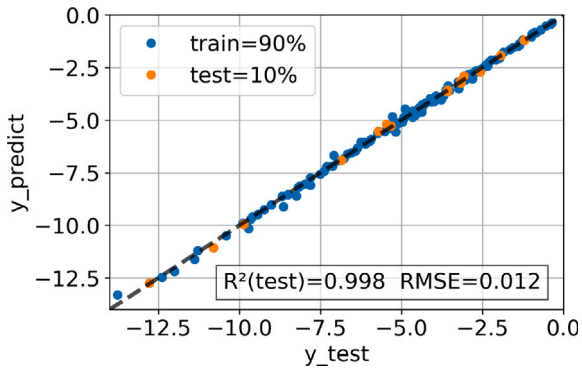

Fig. 8. Training vs. Test Data of the 2D ANN.

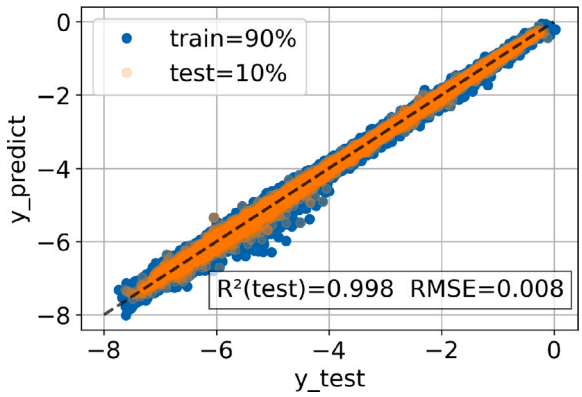

Fig. 9. Training vs. Test Data of the 6D ANN.

the AK methods, an arbitrary Gaussian function centred on (U=25, σ_U=2.5) has been added to the damage predicted by the 2D ANN, still in the (U, σ_U) space: The effect of the Gaussian function on the partial damage variations is clearly visible by its red spot on the left-hand side graph of Fig. 10. On the right-hand side graph of Fig. 10, damage variations are displayed with a logarithmic scale to improve its visibility: it corresponds to the 2D pdf displayed on Figs. 5 and 11 with a linear scale.

4.2. Sequential enrichment

Three criteria have been suggested for this study: an uncorrelated approach, AK-DA, and MAKSUR, described respectively in Section 2.2, 2.3 and 2.4. For the three approaches, the implementation described below is chosen.

4.2.1. Implementation

For the AK strategy, the Kriging implementation of the OpenTURNS Python package [64] is used with a constant trend and an anisotropic 5/2-Matérn covariance kernel which is a flexible kernel and suited for the expected smoothness of the damage.

To compare the different criteria with a sequential enrichment, during each cycle of enrichment, only one new point is added to the previous DoE ($n_{enr} = 1$). The hyperparameters are updated at each calibration of the Kriging model. The points of the successive DoEs are standardized and each hyperparameter is selected in $[10^{-5}, 10]$ using the multistart Truncated Newton Constrained solver implemented in OpenTURNS from 20 initial points. This configuration enables to obtain good hyperparameters within a reasonable time.

The cycles of enrichment end when the coefficient of variation $C.o.V_{MC}$ defined in Eq. (8) goes below 1% which is considered sufficiently accurate.

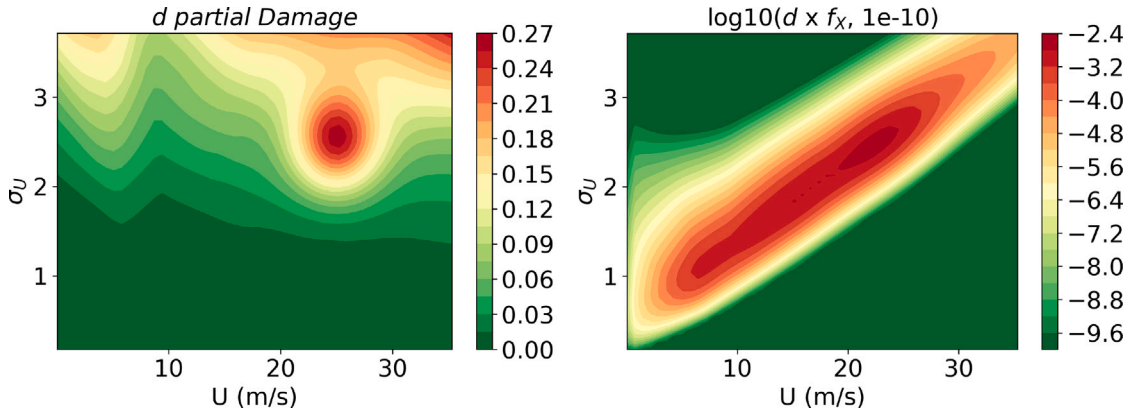

Fig. 10. Damage $d(x)$ (left graph) and occurring damage $d \times f_X$ on a log scale (right graph).

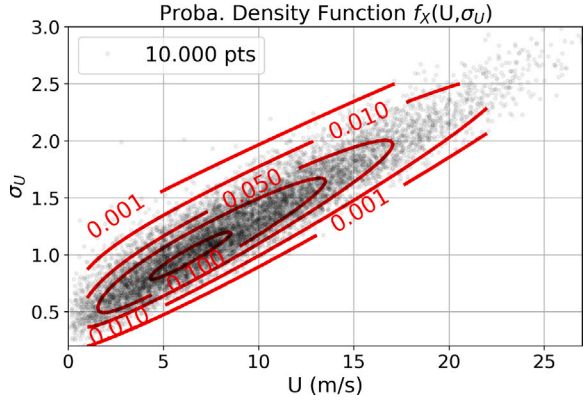

Fig. 11. Contour plot of the pdf f_X(U, σ_U) and Monte Carlo sample of 10.000 points.

To analyse the sensitivity to the initial DoE, 10 initial DoEs are built. These DoE are maximin LHS [65,66] of 20 points. This maximin LHS is a simple sampling method that optimizes the coverage of the 2D domain and is therefore well suited to calibrate the initial kriging model. Moreover, considering a sample of size 10 times the dimension of the input space usually provides a good initial DoE. This results in 30 analyses: a analysis corresponding to the estimation of the total damage using one of the three enrichment criteria from one of the ten initial DoEs.

A Monte Carlo sample of $n_{MC} = 10.000$ points is obtained from the 2D probability density function f_X (Fig. 11) which is used in the enrichment procedure. The total damage is then approximated by D_{MC}(2) where d is replaced with the ANN described in Section 4.1 and we obtain $D_{MC} = 0.01405$. This reference value will be used to compare the different enrichment strategies.

4.2.2. Numerical results

Table 4 gathers the results of the 30 analyses. Each column corresponds to an indicator of performance: the first one is the estimated damage which corresponds to $\mathbb{E}\left[\widetilde{D}_{MC}\right]$, the second one is the number of cycle of enrichment needed to complete the method and finally the error in percentage between the estimation $\mathbb{E}\left[\widetilde{D}_{MC}\right]$ and the damage of reference D_{MC}. For each approach (each row), the mean over the ten analyses (i.e. from the ten different initial DoEs) of each indicator is given as well as the extreme values (i.e. min–max values).

Fig. 12 shows the evolution of the total damage estimation (left graph) and of the variance of the estimator (right graph), during the 18 first cycles of enrichment starting. The whiskers represent the variability due to the choice of the initial DoE. More precisely, the whiskers cover the min–max range, the boxes extend from the first quartile to the third quartile with a line at the median.

All methods have converged to the total damage D_{MC} (Table 4 and left graph of Fig. 12). We can notice that a few Kriging results give very high reference damage log values, basically around 1.3 at cycles 6, 9 and 12 indeed the Gaussian function increases the model complexity and makes it difficult to optimize Kriging hyperparameters. The issue disappears in the following cycles, with the addition of new points. MAKSUR approach has the fastest convergence speed with the lowest number of enrichment cycles, on average 22 (Table 4) with always the lowest total damage variance for cycles higher than 6 (green box plots on the right graph of Fig. 12). To obtain the same precision, the uncorrelated and AK-DA criteria need respectively on average 180.9 and 31.1 cycles of enrichment.

4.3. Multipoint enrichment

To further analyse the behaviour of the different criteria, the multipoint version of AK-DA and MAKSUR are also implemented.

4.3.1. Implementation

The implementation of the methods described in Section 4.2.1 is conserved except that 5 enrichment points are added during each enrichment cycle ($n_{enr} = 5$).

As mentioned in Section 2.3, the parameter r involved in the AK-DA multipoint criterion is difficult to choose a priori. To study the sensitivity of this criterion to r, two different and reasonable values are considered here: $r = 0.3$ and $r = 0.9$.

4.3.2. Numerical results

The results are displayed in Table 5 and Fig. 13.

Although during the first few enrichment cycles, the choice of initial DoE has a large influence on the damage estimate, after four cycles we see that all analyses provide a good approximation of the total damage.

On average, MAKSUR criterion stops after 5.1 cycles. With $r = 0.3$, AK-DA stops after 7.6 cycles and is more restrictive than AK-DA with $r = 0.9$ in term of candidate points which gives worse results.

A comparison of the third and fifth enrichment cycles between MAKSUR and AK-DA $r = 0.3$ criteria are displayed on Figs. 14 and 15. For the 1st and 2nd cycle of enrichment MAKSUR and AK-DA select approximately the same points. At the 3rd enrichment cycle, the zone of interest, which corresponds to the maximum damage area ($log10(d \times f_X) = -2.4$) around the Gaussian function centre is reached by several MAKSUR points. At the 5th enrichment cycle, the solution is fully recovered by MAKSUR: Fig. 15 matches perfectly the solution (Fig. 10). AK-DA criterion needs two more enrichment cycles to recover the solution (Table 5).

Table 4
Results of MAKSUR, AK-DA and an uncorrelated criteria for the 2D case from an initial DoE of n_0=20 points with n_{enr} = 1 point per cycle.

	Damage estimation $\mathbb{E}\left[\widetilde{D}_{MC}\right]$	# cycles of enrichment	Error (%)
uncorrelated	0.01405 [0.01403–0.01406]	180.9 [104–299]	0.08 [0.01–0.15]
AK-DA	0.01394 [0.01360–0.01414]	31.1 [23–41]	0.91 [0.03–3.25]
MAKSUR	0.01405 [0.01387–0.01444]	22.0 [18–26]	1.01 [0.30–2.76]

Table 5
Results of MAKSUR and AK-DA for the 2D case from an initial DoE of $n_0 = 20$ points with $n_{enr} = 5$ points per cycle.

	Damage estimation $\mathbb{E}\left[\widetilde{D}_{MC}\right]$	# cycles of enrichment	Error (%)
AK-DA r = 0.3	0.01401 [0.01386–0.01407]	7.6 [5–9]	0.38 [0.00–1.41]
AK-DA r = 0.9	0.01401 [0.01376–0.01408]	9.5 [8–11]	0.45 [0.04–2.11]
MAKSUR	0.01412 [0.01400–0.01427]	5.1 [3–7]	0.68 [0.15–1.55]

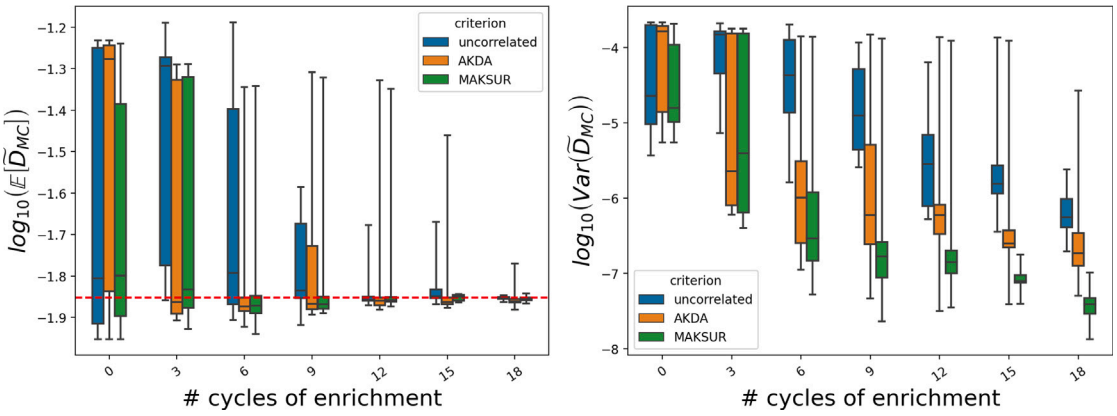

Fig. 12. Evolution of the total damage estimation (left graph) and of the variance of the estimator (right graph), during the 18 first cycles of enrichment starting from an initial DoE of $n_0 = 20$ points with $n_{enr} = 1$ point per cycle. Total damage D_{MC} is plotted by a red dash on the left graph. (For interpretation of the references to colour in this figure legend, the reader is referred to the web version of this article.)

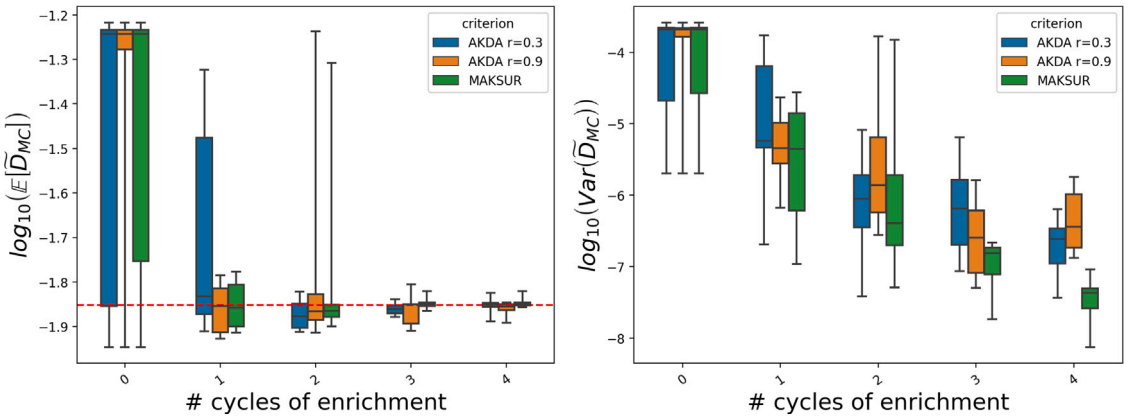

Fig. 13. Evolution of the total damage estimation (left graph) and of the variance of the estimator (right graph), during the four first cycles of enrichment starting from a DoE of $n_0 = 20$ points with $n_{enr} = 5$ points per cycle. Total damage D_{MC} is plotted by a red dash on the left graph. (For interpretation of the references to colour in this figure legend, the reader is referred to the web version of this article.)

5. Application to a realistic floating wind turbine case study

To illustrate the performance of the AK fatigue criteria introduced in the previous sections, let us now consider in this section the complete 6D problem for the damage at the top of the FOWT mooring line which was detailed in Section 3. To fasten the computations, we use the 6D surrogate neural network presented in the same section. This simplifications has no consequence on the result interpretation as we will consider the cost performance as the number of calls to the ANN.

In this section we will compare the multipoint version of AK-DA (for $r = 0.5$ and $r = 0.9$) and MAKSUR.

5.1. Implementation

The implementation of the methods described in Section 4.2.1 is conserved except that during each cycle of enrichment, 10 new enrichment points are added to the previous DoE ($n_{enr} = 10$) to observe how the criteria perform when we increase the number of enrichment points per cycle.

Here again, the analysis are repeated from a set of 10 different initial DoEs leading to 30 analysis (10 per criterion). Since the input space is in 6D, the initial DoEs are composed of 60 points.

The resolution of problems (11) and (16) during the MAKSUR and AK-DA approaches require to evaluate the covariance of $\widetilde{d}$ between

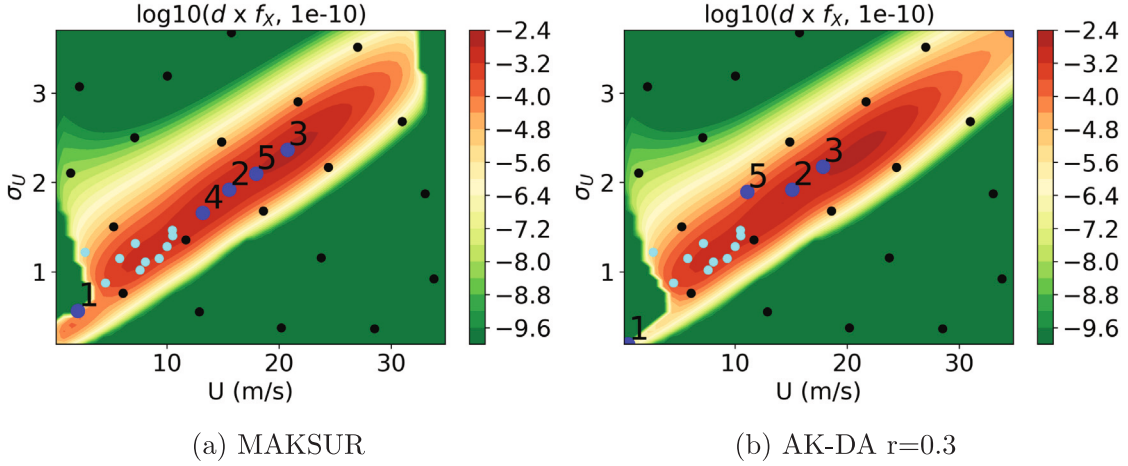

Fig. 14. Comparison between MAKSUR and AK-DA $r = 0.3$ at the 3th cycle of enrichment. The initial DoE is made of $n_0 = 20$ black points. Points of the 1st and 2nd enrichment cycles are in light blue. Points of the current enrichment cycle are numbered in dark blue. (For interpretation of the references to colour in this figure legend, the reader is referred to the web version of this article.)

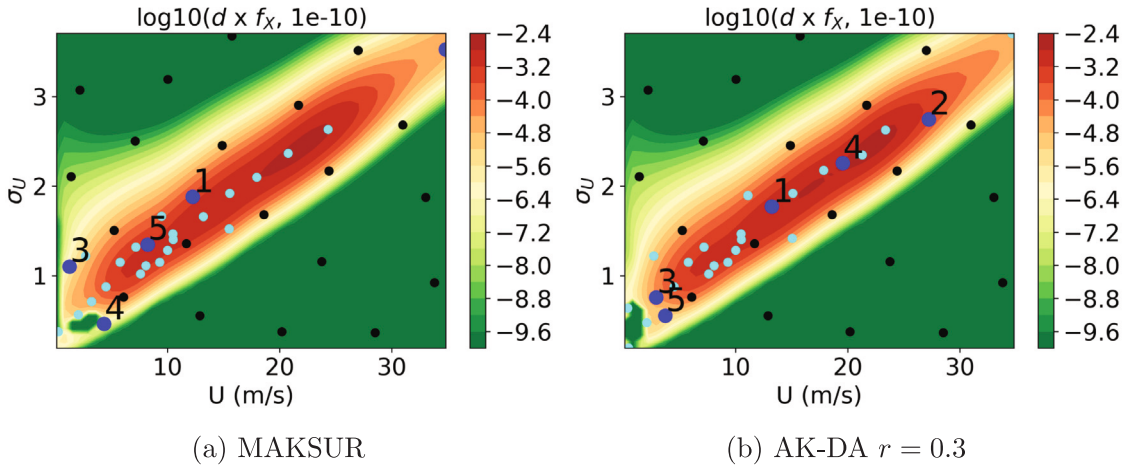

Fig. 15. Comparison between MAKSUR and AK-DA ($r = 0.3$) at the 5th cycle of enrichment. The initial DoE is made of $n_0 = 20$ black points. Points of the 4 1st enrichment cycles are in light blue. Points of the current enrichment cycle are numbered in dark blue . (For interpretation of the references to colour in this figure legend, the reader is referred to the web version of this article.)

every point of $\mathbb{X}_{MC}$. This is very time consuming when considering a large sample size of the Monte Carlo sample despite any call to the multiphysics simulator is needed. To reduce the computation time, a subsample of 10000 points of $\mathbb{X}_{MC}$ is considered and denoted $\mathbb{X}_{MC,s}$. For AK-DA, problem (11) is replaced with

$$x_{enr} = \underset{x_c \in \mathbb{X}_c}{\operatorname{argmax}} \left| \sum_{x' \in \mathbb{X}_{MC,s}} c\left(x_c, x'\right) \right| \tag{20}$$

where, for the first iteration, $\mathbb{X}_c = \mathbb{X}_{MC,s}$ (instead of $\mathbb{X}_{MC}$). For MAKSUR, problem (16) is replaced with

$$x_{enr} = \underset{x_c \in \mathbb{X}_{MC,s}}{\operatorname{argmax}} \left(a_1, \ldots, a_n, a_{x_c}\right)^T \Sigma^{-1}_{\mathbb{D}_{x_c}} \left(a_1, \ldots, a_n, a_{x_c}\right) \tag{21}$$

where for all i we have $a_i = \sum_{x \in \mathbb{X}_{MC,s}} c(x_{(enr,i)}, x)$ and $a_{x_c} = \sum_{x \in \mathbb{X}_{MC,s}} c(x_c, x)$.

To avoid potential bias, at the beginning of every new cycle of enrichment, these 10 000 points are resampled randomly among the full Monte Carlo sample.

Finally, since in this case we used the ANN, d is nearly instantaneous to evaluate and the true total damage D_{MC} defined in Eq. (2) is estimated with a large Monte Carlo sample of 60453 points such that $D_{MC} = 0.00890$. This damage is used as reference to compare the different enrichment approaches. Note that this reference value is close to that obtained with the real simulator, D_{ref} at the end of Section 3, with a relative error of about 6.6%. This approximation comes from the ANN regression illustrated in Fig. 9.

5.2. Numerical results

Table 6 gathers the results of the 30 analyses.

We observe that all the methods provide good estimations of the damage of reference (with a largest error at 3.04% for one analysis with MAKSUR). However, MAKSUR requires much less evaluations of d to reach a given precision. Indeed, in average only 17.7 cycles of enrichment are performed with MAKSUR whereas 37.2 and 60.0 are needed respectively for AK-DA with $r = 0.5$ and $r = 0.9$. This also highlights the importance of the parameter r in AK-DA which has to be chosen a priori by the user.

To further analyse the behaviour of the different methods, we display in Fig. 16 the results of the 9 first cycles for each enrichment approach (the whiskers correspond to the variation over the 10 analyses). The figure on the left indicates the evolution of the logarithm of the estimated damage ($\log_{10}\left(\mathbb{E}\left[\widetilde{D}_{MC}\right]\right)$). The red dotted line corresponds to the damage of reference. The figure on the right shows the evolution

Table 6
Results of MAKSUR and AK-DA for the 6D case with $n_{enr} = 10$.

	Damage estimation $\mathbb{E}\left[\widetilde{D}_{MC}\right]$	# cycles of enrichment	Error (%)
AK-DA r = 0.5	0.00894 [0.00886–0.00910]	37.2 [30–43]	0.57 [0.03–2.28]
AK-DA r = 0.9	0.00895 [0.00878–0.00908]	60.0 [54–68]	0.92 [0.23–2.06]
MAKSUR	0.00889 [0.00867–0.00917]	17.7 [14–23]	1.40 [0.35–3.04]

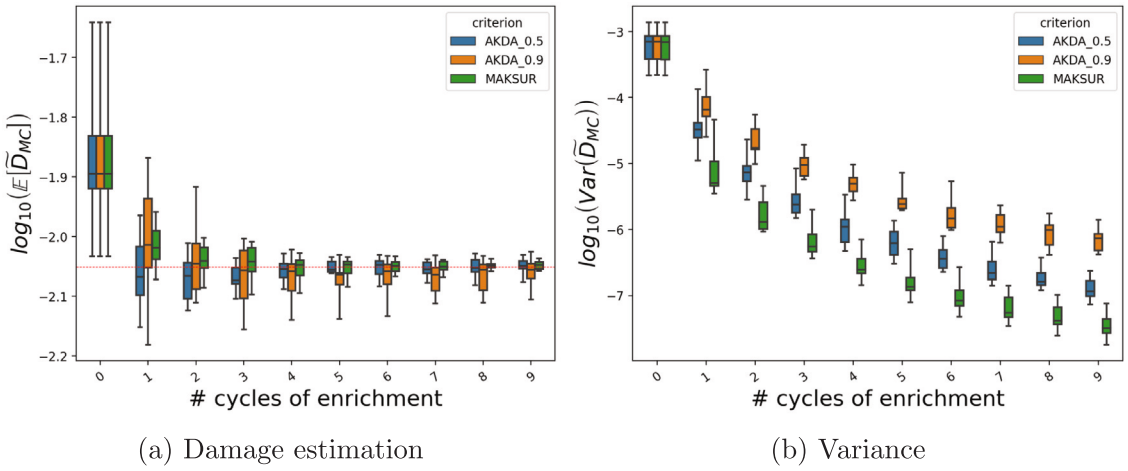

(a) Damage estimation (b) Variance

Fig. 16. Evolution of the damage estimation and of the variance of the estimator during the 9 first cycles of enrichment with $n_{enr} = 10$..

of the logarithm of variance of the estimator ($\log_{10}\left(\mathrm{Var}\left(\widetilde{D}_{MC}\right)\right)$ (this variance is estimated from $\mathbb{X}_{MC,s}$ as explained earlier).

We note that the accuracy of MAKSUR is at least as good as the estimation with the best version of AK-DA. Besides, at the end of each cycle of enrichment, the variance of the estimator is always lower with MAKSUR which implies a smaller uncertainty on the damage estimation. Moreover a significant difference between the two AK-DA methods is observed both for the damage estimation and for the variance of the estimator.

Finally, the analyses in the paper show that the choice of the initial DoE has a small influence compared to the choice of the enrichment criterion. The relative performances of the methods are robust to the choice of the initial DoE.

6. Conclusion

A new method has been presented to compute the mean expectation of pluri-annual fatigue damage for offshore floating wind turbines. This method called MAKSUR for "Mean estimation with AK and a Stepwise Uncertainty Reduction" belongs to the family of AK approaches. However it is specifically suited to compute efficiently the full factorial weighted integral of cumulative damage, accounting for the input variables joint probabilistic distributions. The specificity of MAKSUR relies on the enrichment and stopping criteria employed. MAKSUR adapts the SUR idea [47,67] to integral estimation by selecting iteratively points which maximize the expected variance (including the new points) of the integral derived from the Kriging model of the integrand. On a simplified 2D case, we first demonstrated the efficiency of MAKSUR compared to the AK-DA method of Huchet et al. [46] and to a naive approach for which the enrichment criterion is simply the product of the joint probability of input variables by the variance and the mean of a Kriging on damage. We also shown on a more realistic 6D wind and wave variables floating case study that MAKSUR achieves the same accuracy as the AK-DA method but with a small number of calls to the wind turbine simulator and with a minimum number of parameters to be defined by the user. A reference solution was available for this case study, thanks to a previously computed intensive design of experiments during a supercomputer challenge. MAKSUR converges to a solution close to the reference full factorial damage with only about 237 calls to the simulator which would enable to compute a full factorial estimate of long term damage of offshore wind turbine in industrial context.

A perspective to this work could be to modify the enrichment criterion or the Kriging model in order to account for the positiveness of the damage. To complete the validation, a robustness study should be done with respect to input data. Otherwise, when applying this procedure to a real case of OWT design, one has to extend it for predicting damage at several locations on the structure, accounting for the spatial correlation.

This approach dedicated to mean expectation estimation is however not relevant for cases as Ultimate Limit State design, where the quantity of interest relates to extreme values. It may also require adaptation in special cases such as highly non-stationary output where correlation lengths are very different in different sub-domains of the input space.

Furthermore, the vector of input random parameters X can be extended to a couple of dozen (cf the non exhaustive list of possibilities below Table 1) as long as the curse of dimensionality is not reached making the GP model to difficult to estimate.

Last, let us also mention that the efficiency of this AK method opens the door to more accurate structure design accounting for several sources of uncertainties (see e.g. 37,68 for examples of distributions on material resistance or offshore wind turbine conception). A natural perspective is then to develop new efficient Reliability Based Design Optimization methods like the one suggested in [37], Stieng and Muskulus [69] for fatigue constraints.

CRediT authorship contribution statement

Alexis Cousin: Writing – review & editing, Writing – original draft, Visualization, Methodology, Investigation, Formal analysis. **Nicolas Delépine:** Writing – review & editing, Writing – original draft, Visualization, Resources, Investigation, Data curation. **Martin Guiton:** Writing – review & editing, Writing – original draft, Methodology, Investigation, Formal analysis, Conceptualization. **Miguel Munoz Zuniga:** Writing – review & editing, Writing – original draft, Methodology, Investigation, Formal analysis, Conceptualization. **Timothée Perdrizet:** Methodology, Investigation, Conceptualization.

Declaration of competing interest

The authors declare that they have no known competing financial interests or personal relationships that could have appeared to influence the work reported in this paper.

Data availability

The authors do not have permission to share data.

Acknowledgements

The authors would like to thank people in charge of the Jean Zay machine, the most powerful super-computer dedicated to research in France, owned by GENCI, IDRIS and CNRS. Many thanks to SBM for inspiring the offshore wind turbine case study and IFPEN colleagues for help with DLW calculations and post-processing: Yann Poirette, Guillaume Huwart, Nicolas Bonfils and Vincent Le Corre.

Appendix A. Kriging method (or Gaussian process regression)

The Kriging method relies on the assumption that the expensive function d is a realization of a stationary Gaussian random process $\widetilde{d}_{\text{prior}}$ defined for all $x \in \Omega_X$ as:

$$\widetilde{d}_{\text{prior}}(x) = \sum_{j=1}^{p} \beta_j f_j(x) + Z(x) \tag{22}$$

where the sum $\sum_{j=1}^{p} \beta_j f_j(x)$ defines the trend of the process characterized by the unknown coefficients $\beta_1, \dots, \beta_p$ and the known functions $f_1, \dots, f_p$. Besides, Z is a stationary Gaussian process with zero mean and its covariance function is given by:

$$\mathbb{E}[Z(x)Z(x')] = \sigma^2_{\text{prior}} c_{\text{prior}}(x - x'). \tag{23}$$

The value of p, the functions f_j $(j = 1, \dots, p)$ as well as the function c_{prior} are chosen by the user (the latter can be chosen from a family of parametric correlation functions [33] and is defined by a set of parameters θ). The unknown parameters σ^2_{prior} and θ are called the hyperparameters and characterize the correlation between two points of the process Z. They represent respectively the variance and the correlation lengths of Z.

Let $\mathbb{X}_d = \{x_i, i = 1, \dots, n_{DoE}\}$ be a DoE of Ω_X. We introduce the following notations:

$$f(x) = \left[f_j(x)\right]_{1 \le j \le p}, F = \left[f_j(x_i)\right]_{1 \le i \le n_{DoE}, 1 \le j \le p} \tag{24}$$

$$r_\theta(x) = \left[c_{\text{prior}}(x_i - x)\right]_{1 \le i \le n_{DoE}}, R_\theta = \left[c_{\text{prior}}(x_i - x_j)\right]_{1 \le i \le n_{DoE}, 1 \le j \le n_{DoE}} \tag{25}$$

and m the vector $\left[d\left(x_i\right)\right]_{1 \le i \le n_{DoE}}$.

The DoE and m are used to fit σ_{prior} and θ usually with the cross-validation method or the maximum-likelihood (ML) method [70].

The parameter β can also be estimated within the ML procedure [71] whose solution is given by:

$$\hat{\beta} = \left(F^T R_\theta^{-1} F\right)^{-1} F^T R_\theta^{-1} m. \tag{26}$$

In this context, it is shown that the prediction of the metamodel at a new point x, conditionally to the DoE and m, follows a normal distribution $\widetilde{d}(x) \sim \mathcal{N}\left(\mu(x), \sigma^2(x)\right)$ with:

$$\mu(x) = f(x)^T \hat{\beta} + r_\theta(x)^T R_\theta^{-1}(m - F\hat{\beta}) \tag{27}$$

and

$$\sigma^2(x) = \sigma^2_{prior}\left(1 - r_\theta(x)^T R_\theta^{-1} r_\theta(x) + u_\theta(x)^T \left(F^T R_\theta^{-1} F\right)^{-1} u_\theta(x)\right) \tag{28}$$

with $u_\theta(x) = F^T R_\theta^{-1} r_\theta(x) - f(x)$.

Moreover, for two points x and x', the predictions of the metamodel at these points $\left(\widetilde{d}(x), \widetilde{d}(x')\right)$ is a Gaussian vector such that the covariance $\text{Cov}\left(\widetilde{d}(x), \widetilde{d}(x')\right)$, that we denote $c(x, x')$, is given by the following equation:

$$c(x, x') = \sigma^2_{prior}\left(c_{\text{prior}}(x, x') - r_\theta(x)^T R_\theta^{-1} r_\theta(x') + u_\theta(x)^T \left(F^T R_\theta^{-1} F\right)^{-1} u_\theta(x')\right). \tag{29}$$

Appendix B. Calculation of the posterior variance

We present in this appendix the calculation of the posterior variance involved in the MAKSUR approach. Let $\widetilde{d}$ be the Kriging model of d calibrated at the end of the $k-1$-th cycle of enrichment from the updated DoE $\mathbb{X}_d^{k-1}$. We consider that during the kth cycle, already n iterations were performed (with $n < n_{enr}$) and therefore n enrichment points are already selected : $\mathbb{X}_{enr} = \{x_{(enr,1)}, \dots, x_{(enr,n)}\}$. During the $n+1$-th iteration, the new enrichment point is the solution of:

$$x_{enr} = \underset{x_c \in \mathbb{X}_{MC}}{\text{argmin}} \mathbb{E}_{\mathbb{D}_{x_c}}\left[\text{Var}\left(\widetilde{D}_{MC} | \mathbb{D}_{x_c}\right)\right] \tag{30}$$

where $\mathbb{D}_{x_c} = \{\widetilde{d}(y), y \in \{x_c, \mathbb{X}_{enr}\}\}$ and $\mathbb{E}_{\mathbb{D}_{x_c}}$ stands for the expectation w.r.t. the random vector composed of the $\widetilde{d}(y) \in \mathbb{D}_{x_c}$. The distribution of $\widetilde{d}$ given $\mathbb{D}_{x_c}$ is denoted $\widetilde{d}_{\mathbb{D}_{x_c}}$. We denote c and $c_{\mathbb{D}_{x_c}}$ respectively the covariance functions of $\widetilde{d}$ and $\widetilde{d}_{\mathbb{D}_{x_c}}$ such that $c(x, x') = \text{Cov}(\widetilde{d}(x), \widetilde{d}(x'))$ and $c_{\mathbb{D}_{x_c}}(x, x') = \text{Cov}(\widetilde{d}_{\mathbb{D}_{x_c}}(x), \widetilde{d}_{\mathbb{D}_{x_c}}(x'))$, $\forall x, x' \in \Omega_X$.

Using corollary 1 of Chevalier et al. [52], we have:

$$c_{\mathbb{D}_{x_c}}(x, x') = c(x, x') - C(\mathbb{D}_{x_c}, x)^T \Sigma^{-1}_{\mathbb{D}_{x_c}} C(\mathbb{D}_{x_c}, x') \tag{31}$$

where $C(\mathbb{D}_{x_c}, x)^T = \left(c(x_{(enr,1)}, x), \dots, c(x_{(enr,n)}, x), c(x_c, x)\right)$ and

$$\Sigma_{\mathbb{D}_{x_c}} = \begin{pmatrix} c(x_{(enr,1)}, x_{(enr,1)}) & \dots & c(x_{(enr,1)}, x_{(enr,n)}) & c(x_{(enr,1)}, x_c) \\ \vdots & \vdots & \vdots & \vdots \\ c(x_{(enr,n)}, x_{(enr,1)}) & \dots & c(x_{(enr,n)}, x_{(enr,n)}) & c(x_{(enr,n)}, x_c) \\ c(x_c, x_{(enr,1)}) & \dots & c(x_c, x_{(enr,n)}) & c(x_c, x_c) \end{pmatrix}. \tag{32}$$

We can first notice that the variance term can be written as

$$\text{Var}\left(\widetilde{D}_{MC} | \mathbb{D}_{x_c}\right) = \frac{1}{n^2_{MC}} \sum_{x \in \mathbb{X}_{MC}} \sum_{x' \in \mathbb{X}_{MC}} c_{\mathbb{D}_{x_c}}(x, x')$$

and, according to Eq. (31), does not depend on the random observations $\mathbb{D}_{x_c}$ but only on the associated experimental points $\{x_c, \mathbb{X}_{enr}\}$ such that the expectation in Eq. (30) is not necessary. Then again using Eq. (31), the optimization problem (30) can be reformulated to rely only on the covariance function of $\widetilde{d}$:

$$\begin{aligned} \underset{x_c \in \mathbb{X}_{MC}}{\text{argmin}} \text{Var}\left(\widetilde{D}_{MC} | \mathbb{D}_{x_c}\right) &= \underset{x_c \in \mathbb{X}_{MC}}{\text{argmin}} \frac{1}{n^2_{MC}} \sum_{x \in \mathbb{X}_{MC}} \sum_{x' \in \mathbb{X}_{MC}} c_{\mathbb{D}_{x_c}}(x, x') \\ &= \underset{x_c \in \mathbb{X}_{MC}}{\text{argmax}} \sum_{x \in \mathbb{X}_{MC}} \sum_{x' \in \mathbb{X}_{MC}} C(\mathbb{D}_{x_c}, x)^T \Sigma^{-1}_{\mathbb{D}_{x_c}} C(\mathbb{D}_{x_c}, x') \\ &= \underset{x_c \in \mathbb{X}_{MC}}{\text{argmax}} \left(a_1, \dots, a_n, a_{x_c}\right)^T \Sigma^{-1}_{\mathbb{D}_{x_c}} \left(a_1, \dots, a_n, a_{x_c}\right) \end{aligned}$$

where $a_i = \sum_{x \in \mathbb{X}_{MC}} c(x_{(enr,i)}, x)$ for $i = 1, \dots, n$ and $a_{x_c} = \sum_{x \in \mathbb{X}_{MC}} c(x_c, x)$. Thus, in MAKSUR, the selection of a new enrichment point is done by solving:

$$x_{enr} = \underset{x_c \in \mathbb{X}_{MC}}{\text{argmax}} \left(a_1, \dots, a_n, a_{x_c}\right)^T \Sigma^{-1}_{\mathbb{D}_{x_c}} \left(a_1, \dots, a_n, a_{x_c}\right).$$

References

[1] Wind Europe. "Wind energy in Europe - 2022 Statistics and the outlook for 2023–2027". 2023.
[2] DNV. DNV-ST-0119 standard. Floating wind turbine structures. 2021.
[3] Vorpahl F, Schwarze H, Fischer T, Seidel M, Jonkman J. Offshore wind turbine environment, loads, simulation, and design. WIREs Energy Environ 2013;2:548–70.
[4] Veldkamp D. A probabilistic evaluation of wind turbine fatigue design rules. Wind Energy 2008;11:655–72.

[5] Velarde J, Kramhøft C, Sørensen JD, Zorzic G. Fatigue reliability of large monopiles for offshore wind turbines. Int J Fatigue 2020;134(105487).

[6] Passon P, Branner K. Condensation of long-term wave climates for the fatigue design of hydrodynamically sensitive offshore wind turbine support structures. Ships Offshore Struct 2016;11(2):142–66.

[7] DNV. DNV-OS-J103 standard. Design of floating wind turbine structures. 2013.

[8] IEC. IEC61400-3-2:2019 standard. Wind energy generation systems – part 3-2: Design requirements for floating offshore wind turbines. 2019.

[9] IEC. IEC61400-1:2019 standard. Wind energy generation systems – part 1: Design requirements. 2019.

[10] Müller K, Cheng PW. Validation of uncertainty in IEC damage calculations based on measurements from alpha ventus. Energy Procedia 2016;94:133–45.

[11] Jahani K, Langlois RG, Afagh FF. Structural dynamics of offshore wind turbines: A review. Ocean Eng 2022;251:111136.

[12] Katsikogiannis G, Sørum SH, Bachynski EE, Amdahl J. Environmental lumping for efficient fatigue assessment of large-diameter monopile wind turbines. Mar Struct 2021;77(102939).

[13] Einar L, Stieng S, Muskulus M. Reducing the number of load cases for fatigue damage assessment of offshore wind turbine support structures using a simple severity-based sampling method. Wind Energy Sci 2018;3:805–18.

[14] Zwick D, Muskulus M. Simplified fatigue load assessment in offshore wind turbine structural analysis. Wind Energy 2016;19:265–78.

[15] Murcia JP, Réthoré PE, Dimitrov N, Natarajan A, Sørensen JD, Graf P, et al. Uncertainty propagation through an aeroelastic wind turbine model using polynomial surrogates. Renew Energy 2018;119:910–22.

[16] Wilkie D, Galasso C. Gaussian process regression for fatigue reliability analysis of offshore wind turbines. Struct Saf 2021;88(102020).

[17] Nispel A, Ekwaro-Osire S, Dias JP, A. Cunha Jr. Uncertainty quantification for fatigue life of offshore wind turbine structure. J Risk Uncertain Eng Syst B 2021;7:040901.

[18] Fekhari E, Chabridon V, Muré J, Iooss B. Given-data probabilistic fatigue assessment for offshore wind turbines using Bayesian quadrature. Data-Centric Engineering 2024;5:e5. http://dx.doi.org/10.1017/dce.2023.27.

[19] Barrera C, Battistella T, Guanche R, Losada IJ. Mooring system fatigue analysis of a floating offshore wind turbine. Ocean Eng 2020;195(106670).

[20] Müller K, Dazer M, Cheng PW. Damage assessment of Floating Offshore Wind Turbine using response surface modeling. Energy Procedia 2017;137:119–33.

[21] Asher M, Croke B, Jakeman A, Peeters L. A review of surrogate models and their application to groundwater modeling. Water Resour Res 2015;51(8):5957–73.

[22] Li Y, Ng. S, Xie M, Goh T. A systematic comparison of metamodeling techniques for simulation optimization in decision support systems. Appl Soft Comput 2010;10(4):1257–73.

[23] Razavi S, Tolson BA, Burn DH. Review of surrogate modeling in water resources. Water Resour Res 2012;48(7):1–32.

[24] Østergård T, Jensen R, Maagaard S. A comparison of six metamodeling techniques applied to building performance simulations. Appl Energy 2018;211:89–103.

[25] Moustapha M, Bourinet J-M, Guillaume B, Sudret B. Comparative study of kriging and support vector regression for structural engineering applications. J Risk Uncertain Eng Syst A 2018;4(2).

[26] Dimitrov N, Kelly M, Vignaroli A, Berg J. From wind to loads: wind turbine site-specific load estimation using databases with high-fidelity load simulations. Wind Energy Sci 2018;3:767–90.

[27] Slot RMM, Sørensen JD, Sudret B, Svenningsen L, Thøgersen ML. Surrogate model uncertainty in wind turbine reliability assessment. Renew Energy 2020;151:1150–62.

[28] Stone M. Cross-validatory choice and assessment of statistical predictions. J R Stat Soc Ser B Stat Methodol 1974;36(2):111–47, URL http://www.jstor.org/stable/2984809.

[29] Molinaro AM, Simon R, Pfeiffer RM. Prediction error estimation: a comparison of resampling methods. Bioinformatics 2005;21(15):3301–7. http://dx.doi.org/10.1093/bioinformatics/bti499, arXiv:https://academic.oup.com/bioinformatics/article-pdf/21/15/3301/6236941/bti499.pdf.

[30] Müller K, Cheng PW. Application of a Monte Carlo procedure for probabilistic fatigue design of floating offshore wind turbines. Wind Energy Sci 2018;3:149–62.

[31] Dige N, Diwekar U. Efficient sampling algorithm for large-scale optimization under uncertainty problems. Comput Chem Eng 2018;115:431–54.

[32] Marelli S, Sudret B. An active-learning algorithm that combines sparse polynomial chaos expansions and bootstrap for structural reliability analysis. Struct Saf 2018;75:67–74.

[33] Rasmussen CE. Gaussian processes in machine learning. In: Advanced lectures on machine learning: ML summer schools 2003, Canberra, Australia, February 2 - 14, 2003, TüBingen, Germany, August 4 - 16, 2003, revised lectures. Berlin, Heidelberg: Springer Berlin Heidelberg; 2004, p. 63–71.

[34] Diouane Y, Picheny V, Le Riche R, Di Perrotolo AS. TREGO: a trust-region framework for efficient global optimization. J Global Optim 2023;86(1):1–23. http://dx.doi.org/10.1007/s10898-022-01245-w.

[35] El Amri R, Helbert C, Munoz Zuniga M, Prieur C, Sinoquet D. Set inversion under functional uncertainties with joint meta-models. 2022, URL https://hal-ifp.archives-ouvertes.fr/hal-02986558 working paper or preprint.

[36] Duhamel C, Helbert C, Munoz Zuniga M, Prieur C, Sinoquet D. A SUR version of the Bichon criterion for excursion set estimation. Stat Comput 2023;33(2):41. http://dx.doi.org/10.1007/s11222-023-10208-4.

[37] Cousin A, Garnier J, Guiton M, Munoz Zuniga M. A two-step procedure for time-dependent reliability-based design optimization involving piece-wise stationary Gaussian processes. Struct Multidiscip Optim 2022;65(120).

[38] Fuhg JN, Fau A, Nackenhorst U. State-of-the-art and comparative review of adaptive sampling methods for kriging. Arch Comput Methods Eng 2021;28:2689–747.

[39] Briol F-X, Oates CJ, Girolami M, Osborne MA, Sejdinovic D. Rejoinder: Probabilistic integration: A Role in statistical computation? Statist Sci 2019;34(1):38–42, URL https://www.jstor.org/stable/26771030 Publisher: Institute of Mathematical Statistics.

[40] Chen Y, Welling M, Smola A. Super-samples from kernel herding. In: Proceedings of the twenty-sixth conference on uncertainty in artificial intelligence. UAI '10, Arlington, Virginia, USA: AUAI Press; 2010, p. 109–16.

[41] Huszár F, Duvenaud D. Optimally-weighted herding is Bayesian quadrature. In: Proceedings of the twenty-eighth conference on uncertainty in artificial intelligence. 2012, p. 377–86.

[42] Pronzato L, Zhigljavsky A. Bayesian quadrature, energy minimization, and space-filling design. SIAM/ASA J Uncertain Quant 2020;8(3):959–1011. http://dx.doi.org/10.1137/18M1210332, URL https://epubs.siam.org/doi/10.1137/18M1210332 Publisher: Society for Industrial and Applied Mathematics.

[43] Kanagawa M, Hennig P. Convergence guarantees for adaptive Bayesian quadrature methods. Advances in neural information processing systems, vol. 32, Curran Associates, Inc.; 2019, URL https://proceedings.neurips.cc/paper/2019/hash/165a59f7cf3b5c4396ba65953d679f17-Abstract.html.

[44] Pronzato L. Performance analysis of greedy algorithms for minimising a Maximum Mean Discrepancy. Stat Comput 2022;33(1):14. http://dx.doi.org/10.1007/s11222-022-10184-1.

[45] Zhang B, Cole DA, Gramacy RB. Distance-distributed design for Gaussian process surrogates. Technometrics 2021;63(1):40–52. http://dx.doi.org/10.1080/00401706.2019.1677269.

[46] Huchet Q, Mattrand C, Beaurepaire P, Relun N, Gayton N. AK-DA: An efficient method for the fatigue assessment of wind turbine structures. Wind Energy 2019;1–15.

[47] Bect J, Ginsbourger D, Li L, Picheny V, Vazquez E. Sequential design of computer experiments for the estimation of a probability of failure. Stat Comput 2012;22:773–93.

[48] Melis C, Caille F, Perdrizet T, Poirette Y, Bozonnet P. A novel tension-leg application for floating offshore wind: Targeting lower nacelle motions. In: Proceedings of the ASME 2016 35th International Conference on Ocean, Offshore and Arctic Engineering. 2016.

[49] Delépine N, Bonfils N, Guiton M, Huwart G, Ferrer G, Poirette Y, et al. Accurate estimation of the lifetime of a floating offshore wind turbine by massive aero-servo-hydro-elastic calculation. In: EERA DeepWind 2022 Conference. 2022.

[50] Krige DG. A statistical approach to some basic mine valuation problems on the Witwatersrand. J South Afr Inst Min Metall 1951;52(6):119–39.

[51] Vanem E, Fekhari E, Dimitrov N, Kelly M, Cousin A, Guiton M. A joint probability distribution model for multivariate wind and wave conditions. In: Proceeding of the international conference on offshore mechanics and artic engineering, vol. OMAE2023-101961. 2023, p. 1–16.

[52] Chevalier Clément, Ginsbourger David, Emery Xavier. Corrected kriging update formulae for batch-sequential data assimilation. In: Mathematics of planet earth. Berlin, Heidelberg: Springer Berlin Heidelberg; 2014, p. 119–22.

[53] Krause A, Singh A, Guestrin C. Near-optimal sensor placements in Gaussian processes: Theory, efficient algorithms and empirical studies. J Mach Learn Res 2008;9:235–84.

[54] Porté-Agel F, Bastankhah M, Shamsoddin S. Wind-turbine and wind-farm flows: a review. Bound-Layer Meteorol 2020;174(1):1–59.

[55] Abbas NJ, Zalkind DS, Pao L, Wright A. A reference open-source controller for fixed and floating offshore wind turbines. Wind Energy Sci 2022;7(1):53–73.

[56] Stewart GM, Robertson A, Jonkman J, Lackner MA. The creation of a comprehensive metocean data set for offshore wind turbine simulations. Wind Energy 2015;1151–9.

[57] Joe H. Multivariate models and multivariate dependence concepts. Chapman and Hall; 1997.

[58] Zang Y, Pinder G. Latin hypercube lattice sample selection strategy for correlated random hydraulic conductivity fields. Water Resour Res 2003;39(8):1226.

[59] Müller K, Faerron-Guzmán R, Manjock A. Identification of critical environmental conditions and design load cases. 2018, Deliverable D7.7 of H2020 LIFES50+ project Grant agreement 640741.

[60] Zwick D, Muskulus M. The simulation error caused by input loading variability in offshore wind turbine structural analysis. Wind Energy 2015;18:1421–32.

[61] Niesłony A. Determination of fragments of multiaxial service loading strongly influencing the fatigue of machine components. Mech Syst Signal Process 2009;23:2712–21.

[62] Rinker J. Rainflow counting routine rainflow_v2.py. Duke univ., GPL license. 2015.

[63] Rossi RR. A review of fatigue curves for mooring lines. In: Proceeding of the international conference on offshore mechanics and artic engineering, vol. OMAE2005-67583. 2005, p. 1097–104.
[64] Baudin M, Dutfoy A, Iooss B, Popelin AL. OpenTURNS: An industrial software for uncertainty quantification in simulation. In: Handbook of uncertainty quantification. Springer International Publishing; 2016, p. 1–38.
[65] McKay MD, Beckman RJ, Conover WJ. A comparison of three methods for selecting values of input variables in the analysis of output from a computer code. Technometrics 2000;42(1):55–61.
[66] Santner TJ, Williams BJ, Notz WI, Williams BJ. The design and analysis of computer experiments. Springer; 2018.
[67] Chevalier C, Bect J, Ginsbourger D, Vazquez E, Picheny V, Richet Y. Fast parallel kriging-based stepwise uncertainty reduction with application to the identification of an excursion set. Technometrics 2014;56(4).
[68] Drexler S, Muskulus M. Reliability of an offshore wind turbine with an uncertain S-N curve. J Phys Conf Ser 2021;2018:012014.
[69] Stieng LES, Muskulus M. Reliability-based design optimization of offshore wind turbine support structures using analytical sensitivities and factorized uncertainty modeling. Wind Energy Sci 2020;5:171–98.
[70] Roustant O, Ginsbourger D, Deville Y. DiceKriging, DiceOptim: Two R packages for the analysis of computer experiments by kriging-based metamodeling and optimization. J Statist Softw Art 2012;51(1):1–55. http://dx.doi.org/10.18637/jss.v051.i01, URL https://www.jstatsoft.org/v051/i01.
[71] Helbert C, Dupuy D, Carraro L. Assessment of uncertainty in computer experiments from Universal to Bayesian Kriging. Appl Stoch Models Bus Ind 2009;25(2):99–113.